

Article

Versatile Coordination Polymer Catalyst for Acid Reactions Involving Biobased Heterocyclic Chemicals

Margarida M. Antunes , Ricardo F. Mendes , Filipe A. Almeida Paz  and Anabela A. Valente * 

Department of Chemistry, CICECO—Aveiro Institute of Materials, University of Aveiro, 3810-193 Aveiro, Portugal; margarida.antunes@ua.pt (M.M.A.); rfmendes@ua.pt (R.F.M.); filipe.paz@ua.pt (F.A.A.P.)

* Correspondence: atav@ua.pt; Tel.: +351-234370603

Abstract: The chemical valorization/repurposing of biomass-derived chemicals contributes to a biobased economy. Furfural (Fur) is a recognized platform chemical produced from renewable lignocellulosic biomass, and furfuryl alcohol (FA) is its most important application. The aromatic aldehydes Fur and benzaldehyde (Bza) are commonly found in the slate of compounds produced via biomass pyrolysis. On the other hand, glycerol (Gly) is a by-product of the industrial production of biodiesel, derived from fatty acid components of biomass. This work focuses on acid catalyzed routes of Fur, Bza, Gly and FA, using a versatile crystalline lamellar coordination polymer catalyst, namely $[Gd(H_4nmp)(H_2O)_2]Cl \cdot 2H_2O$ (**1**) [H_4nmp =nitrilotris(methylenephosphonic acid)] synthesized via an ecofriendly, relatively fast, mild microwave-assisted approach (in water, 70 °C/40 min). This is the first among crystalline coordination polymers or metal-organic framework type materials studied for the Fur/Gly and Bza/Gly reactions, giving heterobicyclic products of the type dioxolane and dioxane, and was also effective for the FA/ethanol reaction. **1** was stable and promoted the target catalytic reactions, selectively leading to heterobicyclic dioxane and dioxolane type products in the Fur/Gly and Bza/Gly reactions (up to 91% and 95% total yields respectively, at 90 °C/4 h), and, on the other hand, 2-(ethoxymethyl)furan and ethyl levulinate from heterocyclic FA.

Keywords: biomass; furfural; furfuryl alcohol; glycerol; benzaldehyde; acid catalysis; coordination polymer



Citation: Antunes, M.M.; Mendes, R.F.; Paz, F.A.A.; Valente, A.A. Versatile Coordination Polymer Catalyst for Acid Reactions Involving Biobased Heterocyclic Chemicals. *Catalysts* **2021**, *11*, 190. <https://doi.org/10.3390/catal11020190>

Academic Editor: Raffaella Mancuso
Received: 10 January 2021
Accepted: 22 January 2021
Published: 1 February 2021

Publisher's Note: MDPI stays neutral with regard to jurisdictional claims in published maps and institutional affiliations.



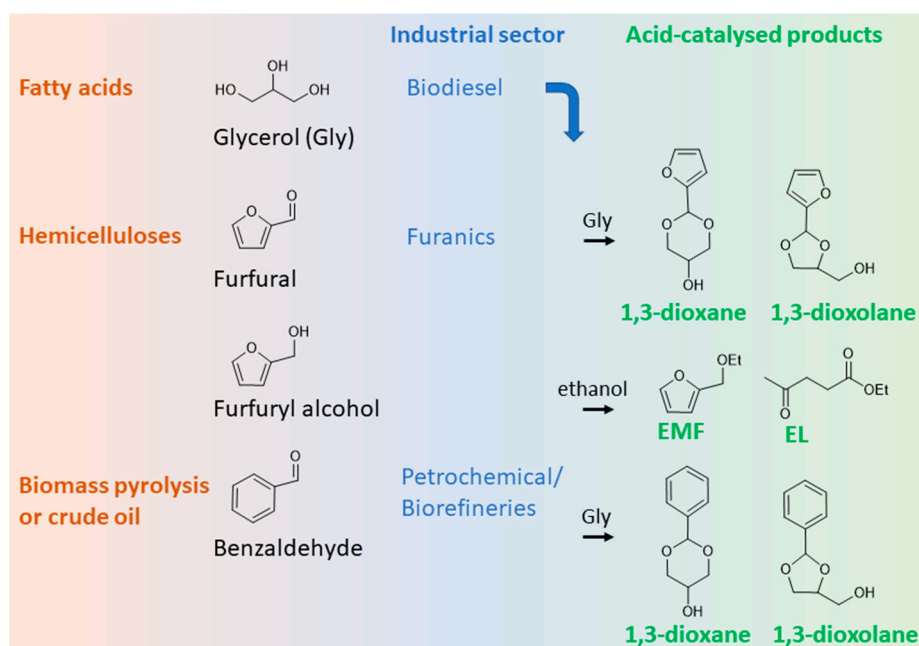
Copyright: © 2021 by the authors. Licensee MDPI, Basel, Switzerland. This article is an open access article distributed under the terms and conditions of the Creative Commons Attribution (CC BY) license (<https://creativecommons.org/licenses/by/4.0/>).

1. Introduction

The conversion of biomass or derived waste/residues/by-products to useful bioproducts may reduce society's dependency on fossil fuels and avoid global warming and energy security issues. A good example concerns glycerol (Gly), a by-product of the biodiesel industry [1]. The biodiesel mandates for transportation fuels imposed by several countries have accounted for uninterrupted supply of Gly with a forecast annual global market growth rate of ca. 4% up to 2027 [1–3]. Gly has increasing demand from food (bakery, processed meat, etc.), cosmetic, personal care, nutraceutical and pharmaceutical industries. Nevertheless, as increasing biofuel production and demand for oleochemicals drive the Gly market growth, it is important to broaden this chemical's portfolio [1,4–8]. Several valorization routes of Gly as feedstock were explored, including reactions of oxidation [4,9–18], carboxylation [19–21], carbonylation [4,22], etherification [23–26], esterification [27–37], transesterification [38–43], hydrogenation [44,45], dehydrogenation [46,47], hydrogenolysis [48–53], oxidehydration [54], dehydration [55–59], polymerization [60–65], aromatization [66], gasification [67,68], reforming [51,69–76], acetalization/ketalization [3,19,31–33,35,37,77–94] and trans-acetalization [95]. The acetalization routes of carbonyl compounds with Gly are particularly important [3,35,94,96] since they may give versatile cyclic acetals (1,3-dioxanes, 1,3-dioxolanes), which are useful bio-based solvents [97,98], starting materials in organic synthesis and protecting group strategies [78,92,93,99], fragrances [78,84,92,99,100], flavors [92,101], cosmetics [84,93,102], pharmaceuticals [84,93,99,102], food and beverage

industries [93,102], polymers [99], surfactants, binders [84,103] and oxygenated fuel additives [3,31,32,35,78,84,87,94,98,99,101,103], among others.

The reactions of Gly with aromatic aldehydes such as furfural (Fur) and benzaldehyde (Bza)—derived from lignocellulosic biomass (Fur) [104], pyrolysis of vegetable biomass (Fur and Bza) [105] or oil (Bza)—may give cyclic acetals (Scheme 1) as fuel additives [77,101,106] with antioxidant, non-toxic and renewable features [84]. Different types of acid catalysts were studied for the Bza/Gly reaction (organic acids [107], metal chlorides [108], ionic liquids [109], Keggin-tungstophosphoric acid-based [92], acid resins [77,79,110] and organic polymers [84], metal or mixed metal oxides [82,111], sulfated metal oxides [33], zeolites [19,79,82], functionalized silicas [93,102,112], mesoporous silicas or aluminosilicates [19,31,32,83,88,113] and silesquioxanes [80]), and for the Fur/Gly reaction (metal chlorides [114], resins [77,106] and organic polymer [84], metal or mixed metal oxides [78,81,99], mesoporous silicas or aluminosilicate (bulk and supported) catalysts [31,32,101,113–115], clays [86,106] and lignosulfonated monolith [103]). Nevertheless, heterogeneous acid catalysts are preferable to homogeneous ones in that the former are easier to store/handle, avoid energy-intensive catalyst separation processes, waste generation and/or corrosion hazards. To the best of our knowledge, the reactions of Fur/Gly and Bza/Gly have not yet been investigated using crystalline coordination polymers or metal organic framework (MOF)-type catalysts, which are versatile hybrid materials.



Scheme 1. The chemical valorization/repurposing of biomass-derived chemicals such as furfural (Fur), furfuryl alcohol (FA) and glycerol (Gly). The reactions of Fur/Gly and benzaldehyde/Gly to useful cyclic acetals, and FA/ethanol to furanic ether (EMF) and levulinate ester (EL).

In this work, the Fur/Gly and Bza/Gly reactions were studied in the presence of $[\text{Gd}(\text{H}_4\text{nmp})(\text{H}_2\text{O})_2]\text{Cl}\cdot 2\text{H}_2\text{O}$ (**1**) [H_6nmp =nitrilotris(methylenephosphonic acid)] (Scheme 1), which is an attractive material in that it may be synthesized via a simple, ecofriendly microwave-assisted approach using water as solvent, and possesses acid properties for catalytic reactions under relatively mild conditions [116]. **1** also proved effective for removing sulfur and nitrogen pollutant compounds from diesel-type mixtures [117].

1 is a (two dimensional) crystalline lamellar coordination polymer with Gd^{3+} centers ($\{\text{GdO}_8\}$ coordination polyhedra) and a flexible organic linker ($\text{H}_4\text{nmp}^{2-}$) (Figure 1) [116]. The organic linker is a zwitterionic species with a protonated central nitrogen atom and peripheral phosphonate groups, each bearing a single negative charge (PO_3H^-). The

phosphonate groups act as μ_2 -O,O' bridging moieties, and P=O and P-OH surface groups are formed. The influence of the reaction conditions and mechanistic and structural features involved in these catalytic systems are discussed based on experimental studies.

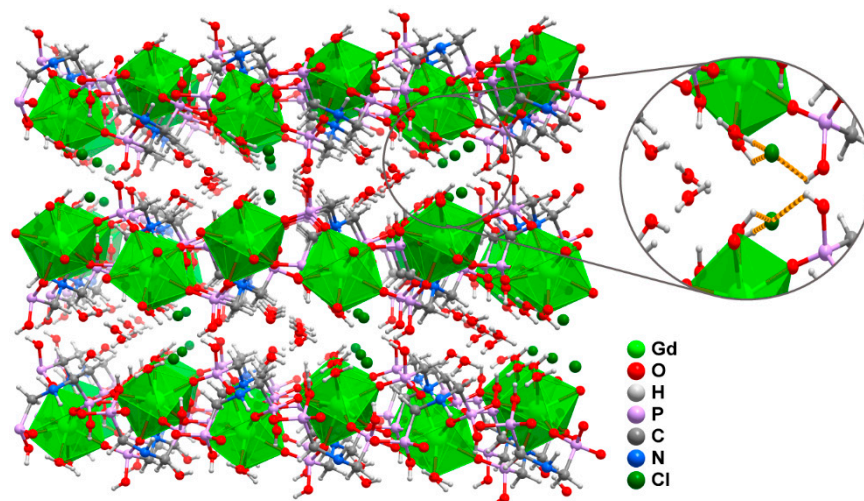


Figure 1. Structural representation of the positively charged crystalline coordination polymer $[\text{Gd}(\text{H}_4\text{nmp})(\text{H}_2\text{O})_2]\text{Cl}\cdot 2\text{H}_2\text{O}$ (**1**).

The catalytic potentialities of **1** were further investigated for converting heterocyclic furfuryl alcohol (FA) to useful bioproducts. FA represents the highest market volume of Fur, produced from lignocellulosic biomass. Fur and FA have wide application profiles [104,118–120]. The reaction of FA with (biomass-derivable) ethanol gives 2-(ethoxymethyl)furan (EMF) and ethyl levulinate (EL) (Scheme 1) [121]. The applications of EMF include bio-solvent [122], pharmaceuticals, food flavor [123–126], aging flavor for beer storage [127–131] or white wine [132] and fuel additive [122,124–126,133–137] since it has a high energy density, cetane number [138] and capacity to reduce soot emissions [124,134,139,140]. On the other hand, EL is an attractive oxygenated fuel extender (its high oxygen content enhances engine efficiency, improves flow properties, etc. [141,142]) with a promising global market [141,143]. Tian et al. [139] reported that EMF and EL present superior antiknock features to Euro95 gasoline, and Lange et al. [144] highlighted the limited footprint CO_2 emissions associated with the use of EMF in fuels. To the best of our knowledge, solely two coordination polymers or MOFs were studied for the conversion of FA to EMF/EL, namely Hf-UiO-66- SO_3H [145] and MIL-101 (Cr)- SO_3H [146,147], both functionalized with sulfonic acid groups.

Hence, **1** is the first of crystalline coordination polymers/MOFs investigated in the Fur/Gly and Bza/Gly reactions, and the first non-sulfonic acid crystalline coordination polymer studied in the FA/ethanol reaction. A relatively fast and mild synthesis protocol of **1**, using water as solvent, is reported. **1** effectively promoted the target biomass-related reactions. The influence of the reaction conditions and insights into the reaction mechanism and catalyst structural features contributing to the formation of the cyclic acetals are reported.

2. Results and Discussion

2.1. General Considerations

The scaled-up synthesis of the hybrid material **1** (Figure 1) was successfully accomplished, as confirmed by powder X-ray diffraction, which was similar to that reported in the literature (Supplementary Figure S1) [117]. Additional characterization studies are discussed in the catalyst stability Section 2.5. Material **1** was explored as an acid catalyst for the reactions of Bza (Section 2.2) and Fur (Section 2.3) with Gly, to give heterobicyclic products. The interest in the repurposing/valorization of Fur, Bza and Gly is related to the

fact that Fur is an established platform chemical industrially produced from lignocellulosic biomass, Gly is industrially associated (as a by-product) with biodiesel production and Fur and Bza are aromatic aldehydes commonly found in the slate of compounds produced via biomass pyrolysis [105,148,149]. **1** promoted the reactions of Fur/Gly and Bza/Gly, leading to the corresponding heterobicyclic products of the type dioxolane and dioxane (five and six membered ring acetals, respectively).

More than 80% of the global Fur produced is converted to furfuryl alcohol (FA) for several industrial sectors [150]. Broadening the applications of these heterocyclic biobased chemicals may positively contribute to a biobased economy. Paving the way in this future direction, the catalytic potential of **1** was herein studied for the acid catalyzed reaction of FA with ethanol to the useful bioproducts 2-(ethoxymethyl)furan (EMF) and ethyl levulinate (EL) (Section 2.6) [121,124,127–131,141,151]. The carbon mass balances closed in at least 96% for the Fur/Gly and Bza/Gly reaction systems, and 89% for the FA/ethanol system.

2.2. Reaction of Benzaldehyde and Glycerol to Heterobicyclic Products

Compound **1** was active for the reaction of Bza with Gly, in the temperature range 50–120 °C, without adding co-solvent, leading mainly to the corresponding dioxolane (five membered ring acetal), namely 2-phenyl-1,3-dioxolan-4-yl)methanol, and dioxane (six membered ring acetal), namely 2-phenyl-1,3-dioxan-5-ol (cis/trans mixture), in high total yields of up to 97% (90 °C, 24 h). Catalyst **1** favored the formation of the dioxane, formed in a molar ratio dioxane:dioxolane of up to 3. The predominance of the dioxane product in the Bza/Gly reaction agrees with the literature [97] for various types of catalysts: MoO_x-TiO₂-ZrO₂ (molar ratio dioxane:dioxolane = 1.13) [111], MoO₃/SiO₂ (1.48) [93], TSA-MCM-48 (1.91) [113] and SO₄²⁻/SnO₂ (1.5) [33]. The temperature and molar ratio Gly:aldehyde are important parameters influencing the catalytic reaction [110]. Hence, the Bza/Gly system was firstly studied in the presence of **1**, using a molar ratio Gly:Bza of 1:2 or 1:3, and a reaction temperature of 90 or 120 °C, 24 h (Table 1). Increasing the molar ratio Gly:Bza from 1:3 to 1:2 led to higher total acetals yield, especially at 90 °C (70% and 97% respectively, at 24 h; entries 1 and 2, Table 1). On the other hand, the total acetals yields were comparable at 90 and 120 °C, using Gly:Bza = 1:2 (97% and 94% yield at 24 h respectively, entries 2 and 4, Table 1). The total acetals yield did not change considerably between 4 and 24 h reaction at 90 °C, likely being thermodynamically limited (95% and 97% respectively, Gly:Bza = 1:2). These results suggested that **1** may favorably operate at reaction temperatures lower than 120 °C, 4 h reaction, using a molar ratio Gly:Bza = 1:2.

Table 1. Influence of the molar ratio Gly:Bza and temperature range 90–120 °C on the Bza/Gly reaction at 24 h, in the presence of **1**.

Entry	T (°C)	Gly:Bza Molar Ratio	Conv. (%)	Product Yield (%)		
				Dioxolane	Dioxane	Total Acetals
1	90	1:3	73	18	52	70
2	90	1:2	99	24	73	97
3	120	1:3	100	28	65	93
4	120	1:2	98	28	66	94

The influence of the catalyst mass load was thus studied using Gly:Bza = 1:2, at 50, 70 and 90 °C, until 4 h reaction (since product yields did not increase considerably after this time) (Figures 2 and 3). In the studied ranges of reaction conditions, the dioxane and dioxolane were always the main products, formed in a molar ratio dioxane:dioxolane in the range 2.0–2.8. For each reaction temperature, a 10-fold increase in the catalyst load from 3.3 to 33 g_{cat} L⁻¹ enhanced the reaction kinetics (Figure 2) and led to higher total acetals yield (Figure 3), e.g., 69% and 79% total yield for 3.3 and 33 g_{cat} L⁻¹ respectively,

at 50 °C/4 h, or 85% and 95% total yield for 3.3 and 33 g_{cat} L⁻¹ respectively, at 90 °C/4 h. Nevertheless, **1** was effective at relatively low temperature in that up to 79% total acetals yield was reached at 50 °C/4 h using only 1 wt.% catalyst (based on Gly).

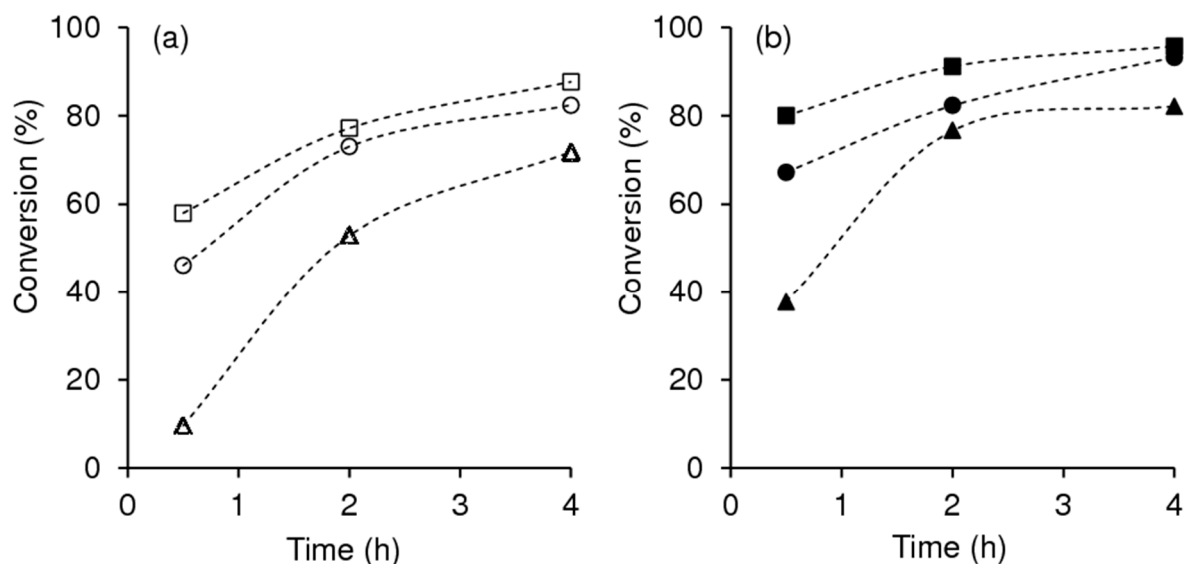


Figure 2. Kinetic profiles of the Bza/Gly reaction in the presence of **1**, at 50 °C (triangles), 70 °C (circles) and 90 °C (squares), using a catalyst load of (a) 3.3 g_{cat} L⁻¹ or (b) 33 g_{cat} L⁻¹.

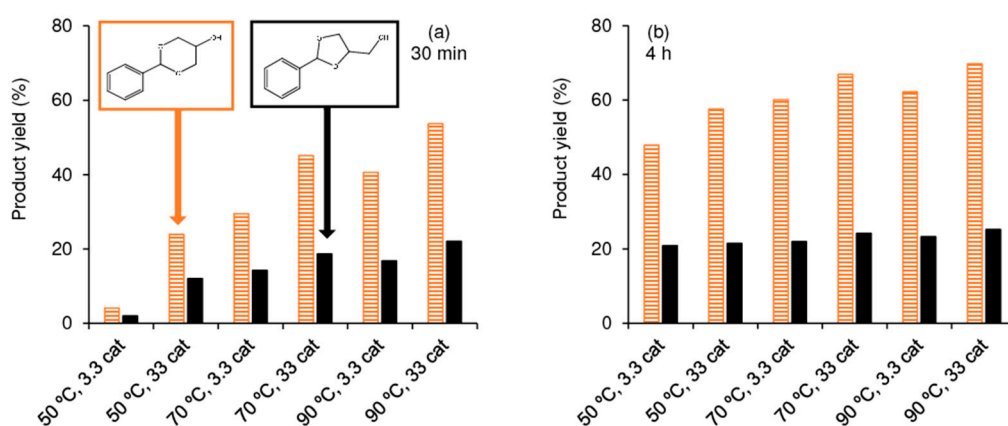


Figure 3. The dioxane (striped bars) and dioxolane (black bars) yields at 30 min (a) and 4 h (b) for the Bza/Gly reaction at 50, 70 and 90 °C using different catalyst mass loads (3.3 or 33 g_{cat} L⁻¹).

Catalyst **1** is, to the best of our knowledge, the first among crystalline coordination polymers/MOF-type materials studied for the Bza/Gly reaction. Table 2 compares the catalytic results for **1** to literature data for different types of solid acid catalysts [19,31–33,77,79,80,82–84,86,88,93,102,110–113]. Under similar reaction conditions to those used by Yamamoto et al. [110] for a cationic resin IRA-120 (entry 7), **1** (entry 6) led to higher acetals total yield and selectivity (51% and 90% total yield for the resin and **1** respectively, at 90 °C/2 h). The sulfonic acid resin Amberlyst-36 led to a higher total acetal yield (94%) than **1** (69%, Figure 3b) under similar conditions (50 and 58.7 °C for **1** and the resin respectively, at 4 h, using a mass ratio catalyst/Gly = 0.01) [79]. Nevertheless, this resin was used with chloroform as a (toxic) solvent, whereas no co-solvent was required for **1**. The performance of **1** seemed to compare favorably to that of the sulfonic acid resin Amberlyst-15 using toluene as a co-solvent (entry 9) [77]. A mixed metal oxide catalyst MoO_x-TiO₂-ZrO₂ led to lower total acetals yield of 32% at 100 °C/0.5 h (entry 10 [111])

than **1** (58% at 90 °C/0.5 h, entry 5), using the same mass ratio catalyst/Gly = 0.01. The metal oxide catalyst MoO₃/SiO₂ tested for the Bza/Gly reaction at 100 °C/8 h using catalyst/Gly = 0.1, led to 72% total acetals yield (entry 11 [93]), and **1**, in the same catalyst/Gly ratio, led to 76% yield at 90 °C/0.5 h (entry 6).

Table 2. Comparison of the results for **1** to literature data for other solid acid catalysts studied for the Bza/Gly reaction to heterobicyclic products ¹.

Entry	Catalyst ² (Solvent)	T (°C)	Gly:Bza (mol)	Cat:Gly (wt)	t (h)	Conv. (%)	Dioxolane Yield (%)	Dioxane Yield (%)	Total Yield (%)	Ref
1	1	50	1:2	0.01	0.5/2	10/53	2/18	4/34	6/52	-
2	1	50	1:2	0.1	0.5/2	38/77	12/52	24/21	38/73	-
3	1	70	1:2	0.01	0.5/2	46/73	14/19	30/51	44/70	-
4	1	70	1:2	0.1	0.5/2	67/82	19/21	45/61	64/82	-
5	1	90	1:2	0.01	0.5/2	58/77	17/22	41/53	58/75	-
6	1	90	1:2	0.1	0.5/2	80/91	22/26	54/64	76/90	-
7	Resin IRA-120	90	1:2	0.1	2	85	nm	nm	51	[110]
8	Amberlyst-36 (chloroform)	59	1.1:1	0.01	4	nm	56	44	94	[79]
9	Amberlyst-15 (toluene)	70	1:1.1	0.06	4	nm	nm	nm	70	[77]
10	MoO _x -TiO ₂ -ZrO ₂	100	1:1	0.01	0.5	32	15	17	32	[111]
11	MoO ₃ /SiO ₂ (toluene)	100	1.1:1	0.1	8	72	29	43	72	[93]
12	Meso-SnO ₂ -T ₃₅₀	100	1:1	0.1	0.5	60	nm	30	30	[82]
13	SO ₄ ²⁻ /SnO ₂	100	1:1	0.05	0.5	80	32	48	80	[33]
14	Beta (Si/Al = 25) (chloroform)	59	1.1:1	0.1	6	nm	41	59	94	[79]
15	Beta (Si/Al = 25)	100	1:1	0.1	0.5	60	nm	29	29	[82]
16	W-Beta (Si/Al = 10)	30	1:1	0.05	1	95	74	21	95	[19]
17	Hf-SBA-15 (<i>t</i> -butanol)	90	1:1	1.09	6	63	15	25	40	[83]
18	Al-SBA-15	100	1:1	0.005	8	72	60	12	72	[32]
19	Al-SBA-15	100	1:1	1.09	8	82	68	14	82	[31]
20	30SiW ₁₂ / MCM-41	30	1:1.2	0.11	1	91	68	23	91	[88]
21	40TSA/ MCM-48	30	1:2	0.05	1	99	34	65	99	[113]
22	POSS-SO ₃ H	30	1:1	0.018	2	90	70	20	90	[80]
23	RHASO ₃ H (toluene)	120	1:2	0.01	8	62	nm	nm	62	[112]
24	An-POP-SO ₃ H	40	1:1	0.217	1.5	78	51	24	75	[84]
25	RHABIm-HSO ₄	120	1:2	0.005	6	54	46	8	54	[102]
26	6BBnU/6	60	2:1	0.05	1	84	50	34	84	[86]

¹ nm = not mentioned, reaction temperature (T) and time (t), molar ratio Gly:Bza, mass ratio catalyst:Gly. ² 40TSA-MCM-48 = 12-tungstosilicic acid (TSA) supported on MCM-48, POSS-SO₃H = synthesized through free radical copolymerization of polyhedral oligomeric vinylsilsesquioxanes (POSS) with sodium *p*-styrene sulfonate, RHASO₃H = rice husk ash (RHA) modified with sulfonic acid groups, An-POP-SO₃H = sulfonic acid functionalized anthracene-derived conjugated porous organic polymer, RHABIm-HSO₄ (consisting of 1-butylimidazole (BIm) supported on rice husk ash via 3-chloropropyltriethoxysilane and then sulphated), 6BBnU/6 (sulfuric acid (6 N, 65 °C, 10 h) activated bentonite clay).

The catalytic performance of **1** compared favorably to that of commercial zeolite H-Beta (entry 14, which in turn was better than zeolites H-ZSM-5 and H-Mordenite, Si/Al = 16–30 [82]) and Hf-SBA-15 (used in a much higher catalyst/Gly mass ratio of 1.09 than that for **1**, entry 17 [83]). Sulfated tin oxide (SO₄²⁻/SnO₂, entry 13) led to 80% total acetals yield at 100 °C/0.5 h (catalyst/Gly = 0.05) [33], and **1** led to a roughly comparable 76% total yield at 90 °C/0.5 h (catalyst/Gly = 0.1, entry 6). Silicotungstate supported on MCM-41 (30SiW₁₂/MCM-41, entry 20 [88]), 12-tungstosilicic acid (TSA) supported on MCM-48 (40TSA-nMCM-48, entry 21 [113]), an oligomeric silsesquioxane functionalized with sulfonic acid groups (POSS-SO₃H, entry 22 [80]) and zeolite Beta loaded with 16.5 wt.% tungsten (entry 16 [19]) led to 90–99% total acetals yield at 30 °C, 1–2 h (catalyst/Gly = 0.018–0.11), while **1** led to 73% total yield at 50 °C/2 h (catalyst/Gly = 0.1, entry 2). A sulfuric acid (6 N, 65 °C, 10 h) activated bentonite clay (6BBnU/6, entry 26 [86]) led to somewhat comparable results to **1**: 84% total acetals yield at 60 °C/1 h,

catalyst/Gly = 0.05, versus 70–82% total yield for **1**, at 70 °C/2 h (catalyst/Gly = 0.01–0.1, entries 3, 4). Sulfonated silica studied in the Bza/Gly reaction with toluene as solvent (RHASO₃H, entry 23 [112]) led to 62% total acetals yield at 120 °C/8 h, whereas **1** led to similar yield (70%, entry 3) at 70 °C/2 h, using the same catalyst/Gly mass ratio of 0.01. In summary, **1** seemed to stand on a relatively good footing compared to the reported commercial catalysts (resins, zeolites), and on a comparable good footing to various types of catalysts prepared at the lab-scale for the Bza/Gly reaction.

2.3. Reaction of Furfural and Glycerol to Heterobicyclic Products

The reaction of Fur/Gly was studied in the presence of **1**, in the temperature range 50–90 °C, using a molar ratio of Gly:Fur of 1:2 and different catalyst mass loads (Figures 4 and 5). The reaction products were the five- (1,3-dioxolane) and six- (1,3-dioxane)-membered ring products, namely 2-(furan-2-yl)-1,3-dioxolan-4-yl)methanol and 2-(furan-2-yl)-1,3-dioxan-5-ol, formed in dioxolane:dioxane molar ratios in the range 1.5–2.5 (at 4 h) for catalyst mass loads in the range 0.38–76 g_{cat} L⁻¹. Kinetic curves were measured for intermediate catalyst mass loads of 3.8 and 38 g_{cat} L⁻¹, at the different reaction temperatures (Figure 4). Conversion increased significantly until 4 h, and only slightly between 4 and 24 h, somewhat in parallel to literature data [78], e.g., conversion at 30 min/4 h/24 h was 48%/74%/82% at 50 °C, and 74%/93%/96% at 90 °C (using 38 g_{cat} L⁻¹, Figure 4b). Without catalyst, conversion was 36% at 90 °C/4 h.

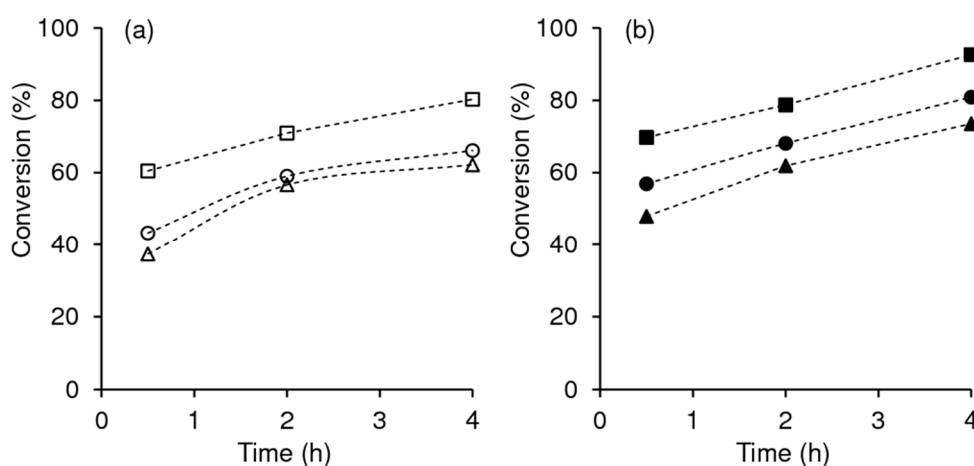


Figure 4. Kinetic profiles for the Fur/Gly reaction in the presence of **1**, at 50 °C (triangles), 70 °C (circles) or 90 °C (squares) using a catalyst load of (a) 3.8 g_{cat} L⁻¹ or (b) 38 g_{cat} L⁻¹.

Increasing the reaction temperature and/or the catalyst mass load enhanced the reaction kinetics (Figure 4) and the total acetals yields until 4 h reaction (Figure 5). For example, the initial catalytic activity increased in the order 106 mol g_{cat}⁻¹ h⁻¹ (50 °C) < 126 mol g_{cat}⁻¹ h⁻¹ (70 °C) < 157 mol g_{cat}⁻¹ h⁻¹ (90 °C), using 38 g_{cat} L⁻¹. At 90 °C, a high total acetals yield of 93% (dioxolane:dioxane = 2.4) was reached at 4 h using 38 g_{cat} L⁻¹, compared to 73–80% at 50–70 °C (Figure 5c). A two-fold increase in the catalyst amount from 38 to 76 g_{cat} L⁻¹ at 50–90 °C enhanced the initial total acetals yields (at 30 min) but did not significantly influence the catalytic results at 4 h (Figure 5). Noticeably, **1** was fairly active for the Fur/Gly reaction at relatively low temperature of 50 °C, using only 0.1 or 1 wt.% catalyst (relative to Gly), which gave 47% and 61% total acetals yield respectively, at 4 h (dioxolane:dioxane \cong 1.5, 0.38 and 3.8 g_{cat} L⁻¹, Figure 5a).

A literature survey for the Fur/Gly reaction to dioxane/dioxolane products indicated that crystalline coordination polymers/MOFs have not yet been investigated for this reaction. Table 3 compares the catalytic results for **1** (using 3.8 or 38 g_{cat} L⁻¹, at 50–90 °C) to literature data for various other types of solid acid catalysts [31,32,77,78,81,84,86,101,103,106,113–115]. When a work focused on the same

type of catalyst modified in slightly different fashions, the best results reported in that work were chosen to be included in Table 3. Catalyst **1** led to a similar acetals' distribution (47% and 21% yield of dioxolane and dioxane respectively, entry 6) under milder reaction conditions to mesoporous Al-SBA-15 (50% and 24% yield of dioxolane and dioxane respectively, entry 7 [31,32]). However, **1** (entry 6) was used in a tenth of the catalyst/Gly mass ratio compared to Al-SBA-15, a much shorter reaction time (12 and 0.5 h, respectively) and lower reaction temperature (100 and 90 °C, respectively). Mesoporous Fe-Al-SBA-15 used in catalyst/Gly = 0.54 led to 100% total acetals yield at 100 °C/12 h (entry 7 [32]), and an approximate total yield of 91% was reached for **1** used in a fifth of the catalyst/Gly mass ratio, at 90 °C/24 h (entry 6). SBA-15 functionalized with sulfonic acid groups (SBA-15-SC, entry 13 [101]) led to 42% total acetals yield at 40 °C/4 h (catalyst/Gly = 0.05), while **1** led to 56% total yield at 50 °C/2 h (catalyst/Gly = 0.01, entry 1). In that study, a sulfonated montmorillonite (MK-10-SC, entry 12 [101]) was more selective to the cyclic acetals than SBA-15-SC (87% total selectivity at 62% conversion, 40 °C/4 h, for MK-10-SC), and **1** used in a fifth of the catalyst/Gly mass ratio led to at least 98% total selectivity at 62% conversion, 50 °C/4 h (entry 1). Mesoporous aluminosilicate of the type MCM-41 led to 80% total acetals yield at 100 °C/2 h (entry 14 [114]), and **1** at slightly lower temperature of 90 °C/2 h led to 76% total yield (entry 6).

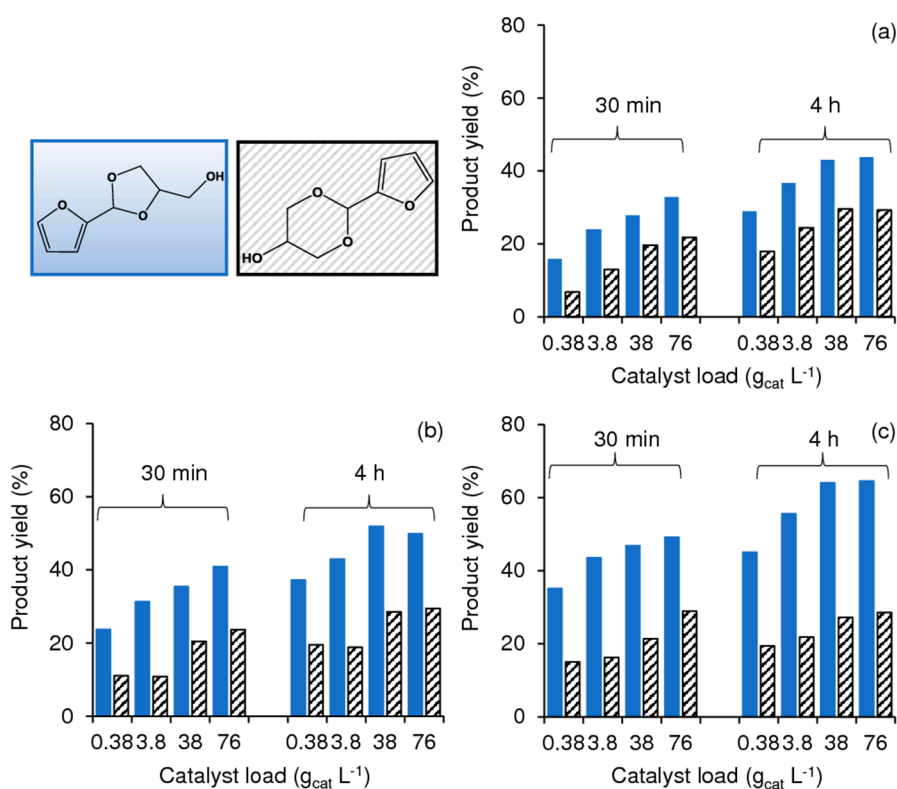
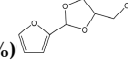
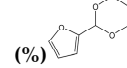


Figure 5. Influence of the catalyst load, reaction temperature and time on the dioxolane (blue bars) and dioxane (striped bars) yields for the Fur/Gly reaction in the presence of **1**, at (a) 50 °C, (b) 70 °C and (c) 90 °C.

Table 3. Comparison of the results for **1** to literature data for other solid acid catalysts studied for the Fur/Gly reaction to heterobicyclic products ¹.

Entry	Catalyst ² (Solvent)	T (°C)	Gly:Fur (mol)	Cat:Gly (wt)	t (h)	Conv. (%)	Dioxolane Yield (%) 	Dioxane Yield (%) 	Total Acetals Yield (%)	Ref
1	1	50	1:2	0.01	0.5/2/4	37/57/62	24/34/36	13/22/25	37/56/61	-
2	1	50	1:2	0.1	0.5/2/4	48/62/74	26/36/43	22/25/30	48/61/73	-
3	1	70	1:2	0.01	0.5/2/4	43/59/66	33/45/46	9/13/16	42/58/62	-
4	1	70	1:2	0.1	0.5/2/4	57/68/81	35/44/52	21/22/29	56/66/81	-
5	1	90	1:2	0.01	0.5/2/4	61/71/80	42/51/63	19/20/15	62/71/78	-
6	1	90	1:2	0.1	0.5/2/4	70/79/93	47/52/64	21/24/27	68/76/91	-
7	Al-SBA-15	100	1:1	1.09	12	74	50	24	74	[31,32]
8	Fe/Al-SBA-15	100	1:1.5	0.54	12	100	60	40	100	[32]
9	Zr-Mont	Rt	1:1	0.10	4	84	52	26	78	[106]
10	6BBNu/6	60	2:1	0.05	1	69	37	32	69	[86]
11	ReHectMw	40	1:1	0.05	4	32	12	11	23	[101]
12	MK-10-SC	40	1:1	0.05	4	62	47	7	54	[101]
13	SBA-15-SC	40	1:1	0.05	4	74	38	4	42	[101]
14	Al-MCM-41	100	1:5	0.1	2	nm	nm	nm	80	[114]
15	TSA-nMCM-48	30	1:2	0.02	0.67	87	37	50	87	[113]
16	H ₃ PW ₁₂ O ₄₀ / MCM-41 (toluene)	>110 ^c	1:1.05	0.05	1.67	nm	nm	nm	89	[115]
17	MoO ₃ /SnO ₂	rt	1:1	0.05	0.5	75	45	26	71	[81]
18	WO ₃ /SnO ₂	rt	1:1	0.05	0.5	67	40	22	62	[81]
19	SO ₄ ²⁻ /SnO ₂	rt	1:1	0.05	0.5	82	55	27	82	[78]
20	An-POP-SO ₃ H	40	1:1	0.2	1.5	85	64	22	85	[84]
21	Amberlyst-15 (cyclohexane)	70	1:1.1	0.06	4	nm	nm	nm	80	[77]
22	Amberlite- IR120	rt	1:1	0.10	4	91	37	19	56	[106]
23	80LS ₂₀ PS ₄₅₀ H ⁺	100	1:2	0.005	1	93	47	46	93	[103]

¹ rt = room temperature, nm = not mentioned, reaction temperature (T) and time (t), molar ratio Gly:Fur, mass ratio catalyst:Gly. ² Zr-Mont = Zr-montmorillonite clay, 6BBNu/6 = sulfuric acid (6 N at 65 °C/10 h)-activated bentonite clay; ReHectMw = rhenium supported on hectorite prepared in a stepwise fashion (aging, ion-exchange) using microwave heating; MK-10-SC = montmorillonite K-10 modified with sulfonic acid groups using chlorosulfonylphenylethyltrimethoxysilane (CSPTMS)/HCl in methylene chloride; SBA-15-SC = sulfonated (using CSPTMS) SBA-15; TSA-nMCM-48 = 12-tungstosilicic acid (TSA) supported on MCM-48; An-POP-SO₃H = sulfonic acid functionalized anthracene (An)-derived porous organic polymer (POP); 80LS₂₀PS₄₅₀H⁺ = protonated lignosulfonate-based macro/mesoporous monolith. ^c Reflux conditions.

A rhenium-containing hectorite ReHectMw used in catalyst/Gly = 0.05 (entry 11 [101]) led to 23% total acetals yield at 40 °C/4 h, and **1** in a fifth of the catalyst/Gly ratio led to 37% total yield at 50 °C/0.5 h. Very good results were reported for Zr-Montmorillonite (entry 9 [106]), 12-tungstosilicic acid supported on MCM-48 (TSA-nMCM-48, entry 15 [113]) and a sulfonic acid functionalized organic polymer (An-POP-SO₃H, entry 20 [84]), used in a catalyst/Gly ratio between 0.02 and 0.2, which led to 78–87% total acetals yield in the temperature range room temperature (rt)–40 °C and 0.5–4 h reaction time. Similar results (78–91% total yield) were reached for **1** with catalyst/Gly = 0.01–0.1, albeit at 90 °C/4 h (entries 5, 6). In relation to some of these catalysts [84], the synthesis of **1** is significantly more simple, not requiring, for example, toxic chlorinated solvents. The tin oxide-based catalysts MoO₃/SnO₂ (prepared in a stepwise fashion involving Mo impregnation and calcination at 650 °C, entry 17 [81], and SO₄²⁻/SnO₂, entry 19 [78]) led to 71–82% total acetals yield at rt/0.5 h (catalyst/Gly = 0.05), while **1** led to a similar result at 50 °C/4 h (catalyst/Gly = 0.1, entry 2). The tungsten/tin oxide WO₃/SnO₂ (entry 18, prepared in a similar fashion to MoO₃/SnO₂ [81]) led to a total acetal yield of 62% at rt/0.5 h (catalyst/Gly = 0.05), which is similar to **1** at 50 °C/4 h used in lower catalyst amount (catalyst/Gly = 0.01, entry 1). Sulfuric acid (6 N at 65 °C/10 h)-activated bentonite clay (6BBNu/6, entry 10 [86]) led to 69% total acetals yield at 60 °C/1 h (catalyst/Gly = 0.05), and **1** led to 73% at 50 °C/4 h (catalyst/Gly = 0.1, entry 2). Protonic lignosulfonate-based macro/mesoporous 80LS₂₀PS₄₅₀H⁺ (synthesized in a multistep fashion involving freeze-dry, pyrolysis, ion exchange) was tested for the Fur/Gly reaction at 100 °C/1 h (entry 23 [103]), leading to similar results

to **1** at 90 °C/4 h, in a higher catalyst:Gly ratio (entry 6), 93% and 91% total acetals yield, respectively. The performance of **1** seemed somewhat comparable/superior to the acid resins Amberlyst-15 (80% total yield at 70 °C/4 h, cyclohexane as co-solvent, entry 21 [77], compared to 81% for **1** at 70 °C/4 h without cosolvent, entry 4) and Amberlite-IR120 (56% total yield at rt/4 h, entry 22 [106], compared to 56% for **1** used in a sixth of the catalyst/Gly mass ratio at 50 °C/2 h, entry 1). Overall, the catalytic results for **1** in the Fur/Gly reaction seemed relatively good among the studied solid acid catalysts.

2.4. Types of Active Species and Mechanistic Insights

The catalytic performance of **1** was compared to that of its synthesis precursors, namely the free organic ligand H_6nmp and the lanthanide oxide Gd_2O_3 , used in equivalent molar amounts to those added with **1** in a normal catalytic run (using $3.8 \text{ g}_{cat} \text{ L}^{-1}$). The free ligand H_6nmp was completely soluble in the reaction media and led the 1,3-dioxolane and 1,3-dioxane products in a total yield of 52% (dioxolane:dioxane = 1.5) at 50 °C/4 h. These results are significant considering that **1** led to 73% total yield under similar conditions. Nevertheless, H_6nmp acted as a homogeneous organocatalyst requiring more demanding catalyst separation processes, in relation to **1**. On the other hand, the lanthanide precursor Gd_2O_3 led to a sluggish reaction (10% conversion at 50 °C/4 h).

The above results suggested that the catalytic activity of **1** seemed to be associated with Brønsted acidity. The attenuated total reflectance (ATR) FT-IR spectra of the fresh and used **1** were similar, and different from those of the catalyst synthesis precursors, H_6nmp and Gd_2O_3 (Figure 6). The fresh and used solids exhibited characteristic bands of the coordinated organic linker and two very weak bands at ca. 1133 and 919 cm^{-1} assignable to $\nu_{as}(PO_2)$ and $\nu_{as}(POH)$ of PO_3H^- groups (which may confer Brønsted acidity) [152].

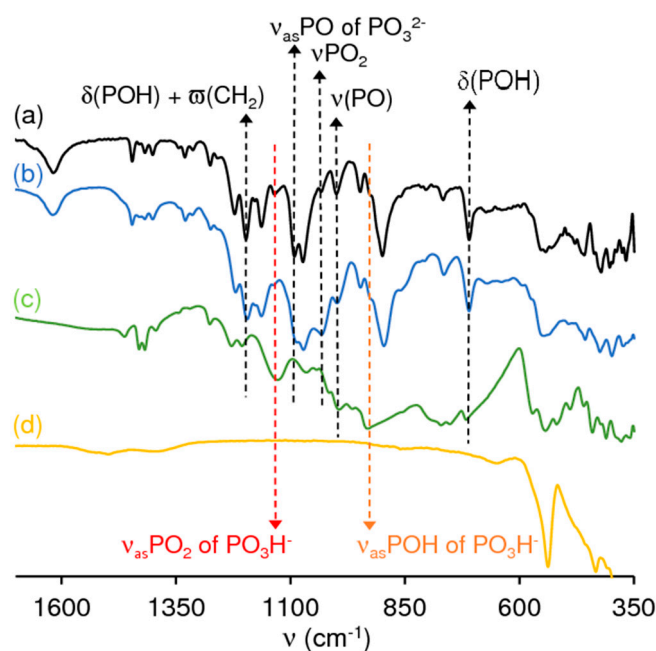
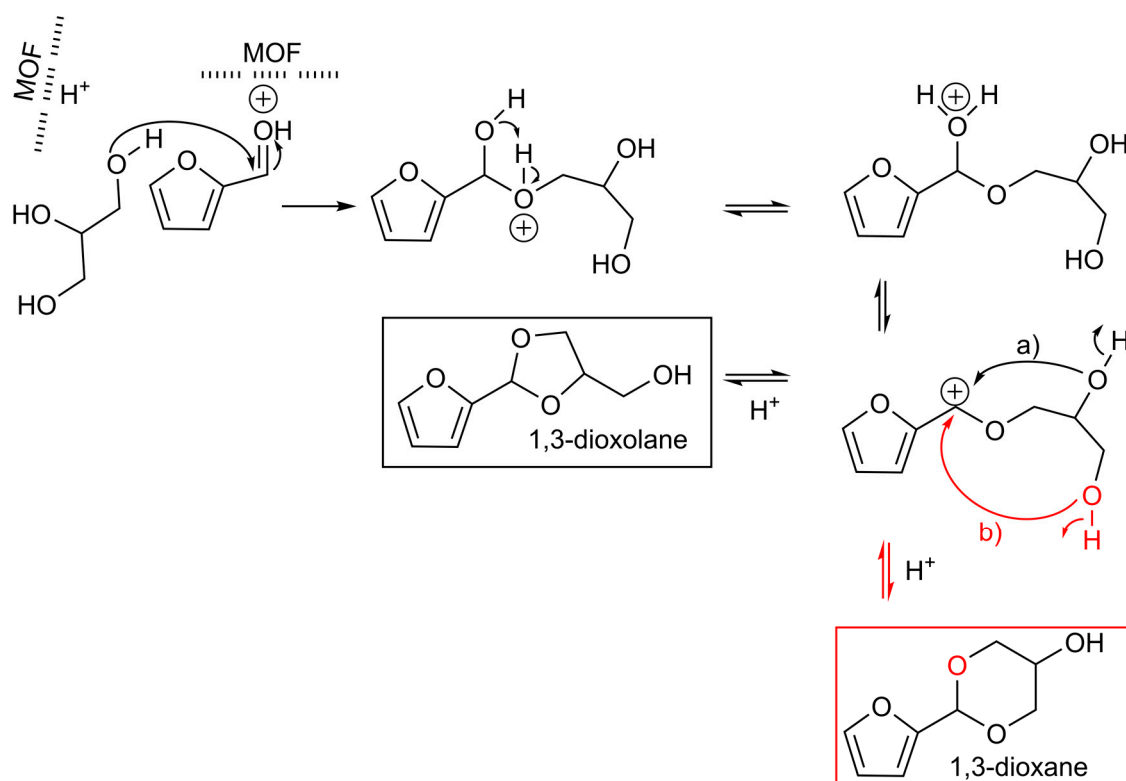


Figure 6. ATR FT-IR spectra of the fresh (a) and used (b) catalyst **1** (Fur/Gly reaction at 50 °C), and the synthesis precursors H_6nmp (c) and Gd_2O_3 (d).

The solids also exhibited a very broad band in the range 3600–3150 cm^{-1} assigned to the $\nu(O-H)$ stretching modes of coordinated water (the solvent used in the catalyst synthesis), a band at ca. 1620 cm^{-1} due to in-plane deformation $\delta(H_2O)$ bands of water molecules and bands in the range 3100–2800 cm^{-1} due to (as)symmetric $\nu(C-H)$ stretching vibrational modes of the linker (Supplementary Figure S2) [153,154].

The catalytic reaction may be triggered by interactions between the oxygen atom of the carbonyl group of the aldehyde reactant and Brønsted acid sites, according to the mechanistic proposal given in Scheme 2 (exemplified for Fur/Gly) [19,113,155]. Specifically, the formation of a hemi-acetal in the reaction of the aldehyde with Gly may be followed by the elimination of a water molecule and formation of a carbocation [79], which, in turn, suffers an attack involving the inner or terminal hydroxyl group of the Gly molecule, finally giving the cyclic acetals 1,3-dioxolane and 1,3-dioxane, respectively.



Scheme 2. Mechanistic proposal exemplified for the Fur/Gly reaction, in the presence of **1**, leading to the 1,3-dioxolane or 1,3-dioxane acetal products.

2.5. Catalyst Stability and Structural Characterization

The stability of **1** was studied using the catalyst for three 4 h batch runs of the Fur/Gly reaction at 50 °C. The catalyst regeneration simply involved washing and drying between runs (details in the Experimental Section 3.2). The conversion and products distribution remained steady in consecutive runs, suggesting that **1** was stable (Figure 7). A contact test (CT) was performed to confirm that the catalytic reaction was heterogeneous. Specifically, Gly was added to the liquid phase of the CT of Fur plus **1** and then left to react (details in the Experimental Section 3.2), which led to 37% conversion at 50 °C/4 h. This result was comparable to that obtained without catalyst (30% at 50 °C/4 h) and considerably inferior to that for a normal catalytic test in the presence of **1** (62–74% conversion, using 3.8–38 g_{cat} L⁻¹), suggesting that the catalytic reaction for **1** is heterogeneous. The molar ratios Gd:P of the fresh and used catalyst were similar (ca. 0.4), consistent with the results of the contact test. The elemental mappings of the fresh and used catalysts indicated uniform distributions of gadolinium and linker (based on phosphorous, Figure 8). No considerable changes in morphology of the fresh and used catalyst occurred, albeit the particle size seemed to have decreased somewhat (Supplementary Figure S3 and Figure 8).

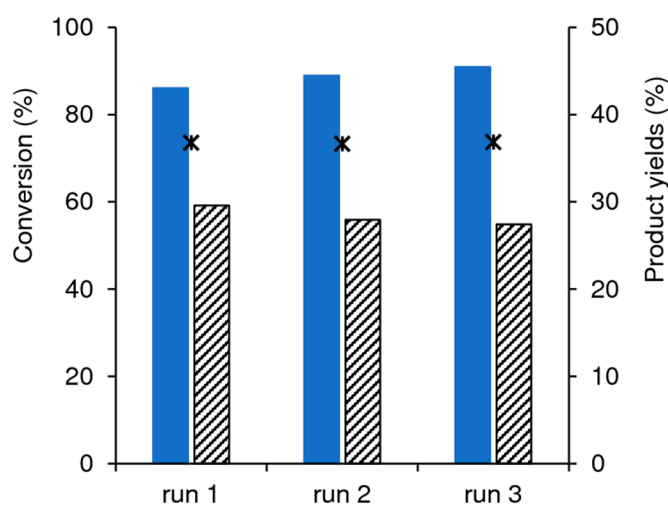


Figure 7. Catalytic performance of **1** in consecutive runs of the Fur/Gly reaction at 50 °C/4 h ($38 \text{ g}_{\text{cat}} \text{ L}^{-1}$), after simple washing/drying: conversion (*) and dioxolane (blue bars) and dioxane (striped bars) yields.

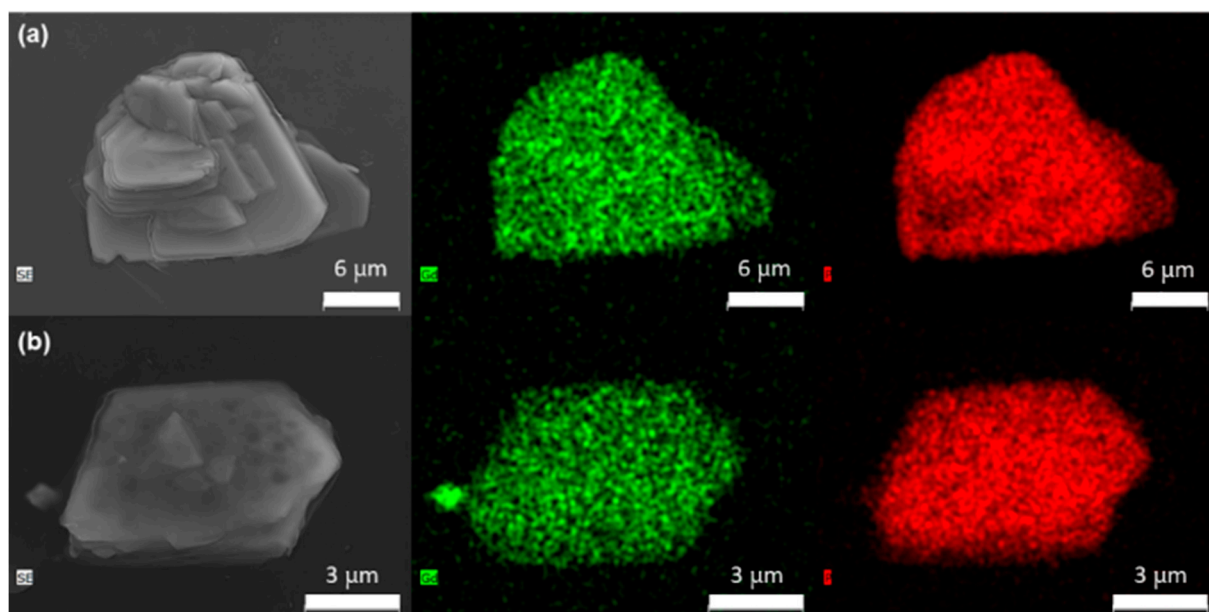


Figure 8. SEM and respective elemental mappings (Gd (green); P (red)) for the fresh (a) and used (b) catalyst **1**.

The powder X-ray diffraction (PXRD) patterns of the fresh and consecutively used solids were similar, suggesting that the crystalline structure of **1** was preserved (Figure 9). The PXRD patterns of the solids recovered from the Fur/Gly reaction at different temperatures (50, 70 and 90 °C) were also similar, suggesting that **1** was thermally stable (Supplementary Figure S4). The ATR FT-IR spectra of the fresh and used solids were comparable, suggesting that the chemical features were essentially preserved during the catalytic reaction (Figure 6 and Supplementary Figure S2).

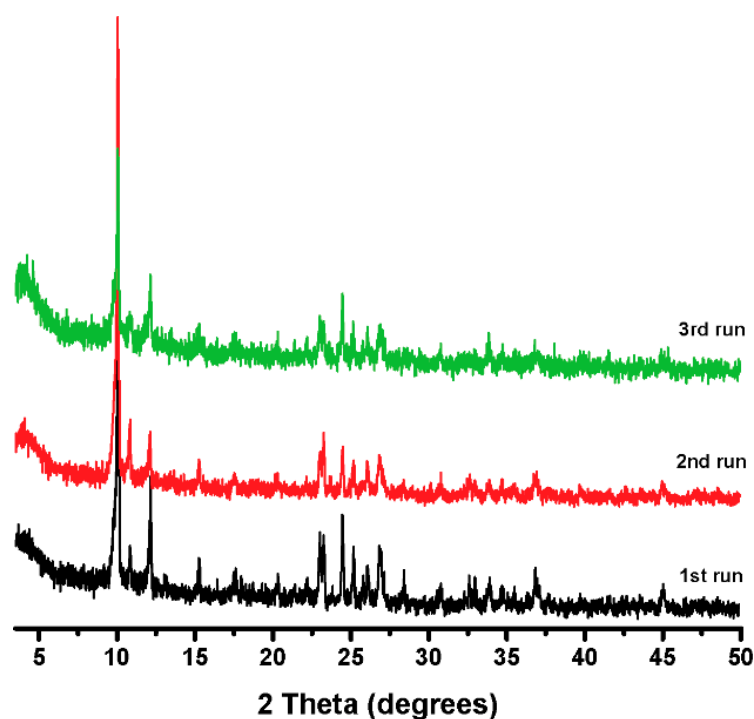


Figure 9. Powder X-ray diffraction patterns of the consecutively used catalyst in the Fur/Gly reaction at 50 °C.

2.6. Other Biobased Systems Involving Heterocyclic Compounds

The catalytic potential of **1** was further explored for the acid catalyzed reaction of heterocyclic furfuryl alcohol (FA) with ethanol (these two reactants are industrially produced from vegetable biomass). The main products were 2-(ethoxymethyl)furan (EMF) and ethyl levulinate (EL), formed in 93% and 95% total yield at 90 and 140 °C respectively, 24 h. FA may be converted to EL via the intermediate formation of the heterocyclic product EMF, which involves furan ring opening promoted by Brønsted acidity [156–158]. For the FA reaction at 140 °C, the EMF yield decreased from 37% at 1 h to 3% at 24 h, whereas EL yield increased from 49% to 92% (Figure 10). Other reaction products included angelica lactone formed in <5% yield. The formation of angelica lactone in the FA/EtOH reaction was reported in the literature for zeolite ZSM-5 as a catalyst [126,159].

The FA reaction at 90 °C in the presence of **1** gave EMF as the main product at 5 h (52% yield) and EL was formed in 25% yield; after 24 h, EMF and EL yields were 35% and 58%, respectively. These results together with those for FA/ethanol at 140 °C indicate that the products' distribution is strongly reaction temperature- and time-dependent.

To the best of our knowledge, only two crystalline hybrid materials were reported in the literature for FA conversion to EMF/EL. Specifically, two MOFs based on hafnium and chromium functionalized with sulfonic (Brønsted) acid groups, namely Hf-UiO-66-SO₃H [145] and MIL-101(Cr)-SO₃H [146,147]. Hf-UiO-66-SO₃H led to a moderate EL yield of 62% at 120 °C/2 h [145], and MIL-101(Cr)-SO₃H [146,147] led to a somewhat comparable EL yield to that for **1**, but under different conditions. Specifically, at 100% FA conversion and 140 °C, the chromium MOF led to 76–79% EL yield at 2 h, whereas **1** led to 72% EL yield at 5 h using a lower catalyst/FA mass ratio (0.3 for **1** versus 0.44–1.02 for the chromium catalyst) and using a more concentrated FA mixture (0.33 M for **1** versus 0.28 M for the chromium catalyst). The total selectivity (EMF plus EL) was higher for **1** (90%) than for MIL-101(Cr)-SO₃H (79%) [146,147]. A detailed comparison of the catalytic results for **1** to literature data for other types of solid acid catalysts is given in the Supplementary Material Section 3 [121,126,134,136,137,145–147,157,160–197]. Overall, the catalytic performance of **1** seemed to stand on an intermediate footing among the various types of solid acid catalysts

reported in the literature for the FA/ethanol system (e.g., commercial zeolites and acid resins, and modified metal oxides). For example, the organocatalyst HCC-ML-SO₃H led to a high EL yield of 85% at 90 °C/8 h [161], albeit it was used in a catalyst/substrate mass ratio three times greater than that for **1** (58% EL yield at 90 °C/24 h). Nano ZSM-5 led to 91% yield at 140 °C/1 h [173], while **1** required 24 h to reach a similar EL yield of 92%, using a similar FA concentration (0.33–0.39 M) but requiring a much lower catalyst/FA mass ratio (0.30 for **1** versus 1.02 for ZSM-5). Superior results were reported for HPW-MesoZSM-5 [193], Ti-HPA [183], Fe-USY [194] and magnetic sulfated zirconia (MSZ) [167], which led to 91–97% EL yield at 120–130 °C and 0.5–5 h (for **1**: 72% EL at 140 °C/5 h). A higher FA initial concentration was used for HPW-MesoZSM-5 and MSZ (1.04–3.12 M versus 0.33 M for **1**) [193], and a lower catalyst/FA mass ratio was used for HPW-MesoZSM5 [193], Ti-HPA [183], Fe-USY [194] and MSZ (0.02–0.07 versus 0.33 for **1**) [167]. However, MSZ requires catalyst regeneration at 500 °C to keep the catalytic performance steady, whereas **1** does not require thermal regeneration.

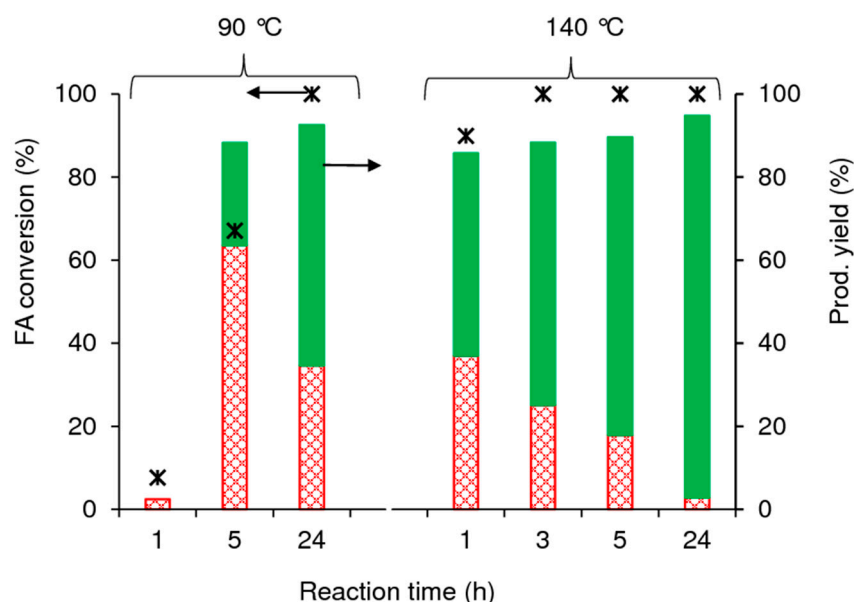


Figure 10. Influence of the reaction temperature and time on FA conversion (*) and the EMF (crossed bars) and EL (solid green bars) yields for the FA/ethanol reaction in the presence of **1**.

3. Materials and Methods

All reagents and solvents were obtained from commercial sources and used as received without further purification, excluding furfural which was distilled prior to use. For the synthesis of [Gd(H₄nmp)(H₂O)₂]Cl·2H₂O (**1**), gadolinium(III) oxide (>99.99%, Jinan Henghua Sci. & Tec. Co. Ltd., Jinan, China), nitrilotris(methylenephosphonic acid) (H₆nmp, N(CH₂PO₃H₂)₃, 97%, Fluka, Algés, Portugal) and hydrochloric acid (HCl, 37% Analytical Reagent Grade, Fisher Chemical, Waltham, MA, USA) were used. For catalytic tests, furfural (Sigma-Aldrich, 99%), benzaldehyde (Sigma-Aldrich, 99%, Algés, Portugal), glycerol (Sigma-Aldrich, ≥99.5%, Algés, Portugal), absolute ethanol (Honeywell, >99.8%, Alfragide, Portugal) and furfuryl alcohol (Aldrich, 99%, Algés, Portugal) were used.

3.1. Catalyst Synthesis and Characterization

The aqueous phase synthesis of [Gd(H₄nmp)(H₂O)₂]Cl·2H₂O (**1**) was based on that previously reported [116], albeit the synthesis was scaled up to give ca. 0.6 g per batch in a relatively fast fashion, specifically, within 40 min under microwave irradiation at 70 °C (75 W power) with stirring (details in the Supplementary Material Section 1).

Powder X-ray diffraction (PXRD) data were collected at ambient temperature on an Empyrean PANalytical diffractometer (Panalytical, Almelo, The Netherlands) (Cu K_{α1,2}

X-radiation, $\lambda_1 = 1.540598 \text{ \AA}$; $\lambda_2 = 1.544426 \text{ \AA}$), equipped with an PIXcel 1D detector and a flat-plate sample holder in a Bragg-Brentano para-focusing optics configuration (45 kV, 40 mA). Intensity data were collected by the step-counting method (step 0.01°), in continuous mode, in the range ca. $3.5 \leq 2\theta \leq 50^\circ$. EDS (energy dispersive X-ray spectroscopy) data was recorded on a high-resolution Hitachi SU-70 (Monocomp, Madrid, Spain) working at 15 kV, employing a Sprit 1.9 EDS microanalysis system, and samples were prepared by deposition on aluminum sample holders followed by carbon coating using an Emitech K950X carbon evaporator. Attenuated total reflectance (ATR) FT-IR spectra were measured on a Mattson-7000 infrared spectrophotometer (Dias de Sousa S.A., Maia, Portugal) equipped with a Specac Golden Gate Mk II ATR accessory with a diamond top plate and KRS-5 focusing lenses.

3.2. Catalytic Tests

The reactions of furfural (Fur) and benzaldehyde (Bza) with glycerol (Gly) were carried out in tubular glass pear-shaped reactors equipped with a TeflonTM-coated magnetic stirring bar and a valve for purging. The batch reactors were loaded with the reactants in a molar ratio Gly: aldehyde of 1:2 or 1:3, and 1 or 10 wt.% catalyst (relative to Gly, which was the limiting reactant). The reaction of furfuryl alcohol (FA, 0.33 M) with ethanol in the presence of **1** ($10 \text{ g}_{\text{cat}} \text{ L}^{-1}$) was carried out using the same type of reactors, at 90 or 140 °C. For comparative purposes, the free linker and gadolinium precursors, namely H_6nmp and Gd_2O_3 respectively, were tested as catalysts, added in an equivalent molar amount to that added together with 1 wt.% (based on Gly) of **1**. The reactor containing the reaction mixture was immersed in a thermostatically controlled oil bath preheated at the desired temperature and stirred at 1000 rpm to avoid diffusional limitations. Blank tests without catalysts were performed for each substrate.

Prior to sampling, after each assay, the reactor was cooled to ambient temperature and the solid catalyst was separated by centrifugation at 10,000 rpm. The analyses were always carried out for fresh samples. The evolution of the catalytic reactions was monitored by gas chromatography (GC) using an Agilent 7820A GC (Soquímica, Porto, Portugal) equipped with a capillary column (HP-5, $30 \text{ m} \times 0.32 \text{ \mu m} \times 0.25 \text{ mm}$) and a flame ionization detector, and product quantification was based on the external calibration. Individual experiments were performed for a given reaction time and the presented results are the mean values of at least two replicates (experimental error < 10%). The product (Prod) yield was calculated relative to the initial amount of the limiting reactant, Gly, using the formula: $100 \times ((\text{molar concentration of Prod at time } t) / (\text{initial molar concentration of Gly}))$. Conversion was based on the limiting reactant Gly. For product identification, a Shimadzu QP2010 ultra-GC-MS (Izasa Scientific, Lisbon, Portugal) equipped with a Phenomenex capillary Zebron ZB5-MS column (ZB-5, $30 \text{ m} \times 0.25 \text{ \mu m} \times 0.25 \text{ mm}$) and He as carrier gas was used, as well as commercial databases Wiley229 and NIST14.

The used catalyst was separated from the reaction mixture by centrifugation at 10,000 rpm, washed with acetone, dried at 85 °C overnight and reused for up to three 4 h batch runs of the Fur/Gly reaction at 50 °C. The contact test (CT) was carried out by heating a stirred suspension of **1** ($3.8 \text{ g}_{\text{cat}} \text{ L}^{-1}$) in Fur at 50 °C for 4 h, under similar conditions to those used for a normal catalytic test, but without Gly. The solid catalyst was separated from the liquid phase by centrifugation at 10,000 rpm and the supernatant liquid phase was passed through a 220 nm pore size PTFE membrane. Gly was added to the solution (filtrate) to give an initial Gly concentration of 4.2 M (as for a normal catalytic test), and this solution was left to react for 4 h at 50 °C, with stirring, and finally analyzed by GC.

4. Conclusions

The hybrid catalyst $[\text{Gd}(\text{H}_4\text{nmp})(\text{H}_2\text{O})_2]\text{Cl} \cdot 2\text{H}_2\text{O}$ (**1**) was synthesized in aqueous phase, in a relatively fast, mild fashion (40 min, 70 °C), in gram-scale. This material proved to be an effective solid acid catalyst for synthesizing heterobicyclic products of the type 1,3-dioxane and 1,3-dioxolane via reactions of biomass-derived furfural (Fur)

and glycerol (Gly), and of benzaldehyde (fossil fuel or biomass derived) and Gly, without requiring co-solvents. The catalyst was stable upon reuse via simple washing/drying procedures, and led to up to 91% total acetals yield in the reaction of Fur/Gly (90 °C, 4 h; molar ratio (2-(furan-2-yl)-1,3-dioxolan-4-yl)methanol)/(2-(furan-2-yl)-1,3-dioxan-5-ol) \cong 2.4), and 95% total acetals yield in the reaction of Bza/Gly (90 °C, 4 h; molar ratio of (2-phenyl-1,3-dioxan-5-ol)/(2-phenyl-1,3-dioxalan-4-yl)methanol) \cong 2.8); at 24 h/90 °C, the total yields increased to 95% and 97%, respectively. To the best of our knowledge, **1** is the first among crystalline coordination polymers or metal-organic framework (MOF)-type materials studied in the literature for these reaction systems. Studies of the influence of the reaction conditions indicated that a lower Gly:Bza molar ratio and increasing the temperature and catalyst load enhanced the total cyclic acetals yields. Insights into the reaction mechanism and catalyst structural features contributing to the formation of cyclic acetals in these acid catalyzed reactions were put forward. Hybrid **1** seemed to perform relatively well based on comparative studies to literature data for various types of solid acid catalysts. Hybrid **1** was further explored for the catalytic conversion of biobased heterocyclic furfuryl alcohol (FA), industrially produced from Fur, which selectively gave ethyl levulinate (up to 92% yield, at 140 °C, 24 h). Decreasing the reaction temperature and time favored the formation of the intermediate 2-(ethoxymethyl)furan (52% yield at 5 h/90 °C). The performance of **1** compared favorably to that reported in the literature for the only two MOFs previously studied for the FA/ethanol conversion (the two MOFs were based on hafnium and chromium functionalized with sulfonic acid groups).

This work included a detailed comparative study of the results for **1** to literature data for different types of catalysts studied for the target reactions. One may envisage that the desired product distributions and superior catalytic performances may be met by exploring the highly versatile (tuneable physicochemical properties) families of crystalline coordination polymers or MOF-type catalysts for these reaction systems.

Supplementary Materials: The following are available online at <https://www.mdpi.com/2073-4344/11/2/190/s1>, detailed synthesis of **1**, Figure S1: Powder X-ray diffraction of [Gd(H₄nmp)(H₂O)₂]Cl·2H₂O (**1**) simulated (black), synthesized using the previously reported synthetic approach (red) and obtained using the scale-up synthesis in this work, Figure S2: ATR FT-IR spectra of the fresh (a) and used (b) catalyst (Fur/Gly reaction at 50 °C), Figure S3: SEM images of [Gd(H₄nmp)(H₂O)₂]Cl·2H₂O (**1**) before (a) and after (b) the catalytic reaction of Fur/Gly at 90 °C, Figure S4: Powder X-ray diffraction of [Gd(H₄nmp)(H₂O)₂]Cl·2H₂O (**1**) after the catalytic reaction of Fur/Gly at different reaction temperatures, Table S1: Comparison of the catalytic results for **1** to literature data for other acid catalysts studied in the FA/ethanol reaction system, and detailed discussion.

Author Contributions: R.F.M. carried out the synthesis of **1** and part of the material characterization (PXRD, EDS), and was responsible for the writing and validation of these results; M.M.A. carried out the catalytic studies and part of the material characterization (FT-IR, SEM, elemental mappings), was responsible for the methodology and validation of the catalytic studies, wrote the original draft and contributed to the revising of this work; F.A.A.P. provided resources for the material's synthesis and characterization, and supervised and validated that work; A.A.V. provided resources and supervised the catalytic studies, and contributed to the conceptualization, writing, revising and editing of the overall work. All authors have read and agreed to the published version of the manuscript.

Funding: This work was developed within the scope of the project CICECO-Aveiro Institute of Materials, UIDB/50011/2020 and UIDP/50011/2020, financed by national funds through the Portuguese Foundation for Science and Technology (FCT)/MCTES. The position held by M.M.A. was funded by national funds (OE), through FCT, I.P., in the scope of the framework contract foreseen in the numbers 4, 5 and 6 of article 23 of the Decree-Law 57/2016 of 29 August, changed by Law 57/2017 of 19 July. R.F.M. gratefully acknowledges FCT for a Junior Research Position (CEECIND/00553/2017).

Data Availability Statement: The compound used for the catalysis and raw characterization data studies herein reported are available from the authors upon request.

Conflicts of Interest: The authors declare no conflict of interest.

References

1. Grand New Research, Glycerol Market Size, Share and Trends Analysis Report by Source (Biodiesel, Fatty Acids, Fatty Alcohols, Soap), by Type (Crude, Refined) by End Use (Food and Beverage, Pharmaceutical), by Region, and Segment Forecasts, 2020–2027. 2020. Available online: <https://www.grandviewresearch.com/industry-analysis/glycerol-market> (accessed on 8 January 2021).
2. ReportLinker, Glycerol Market Size, Share and Trends Analysis Report by Source, by Type, by End Use, by Region and Segment Forecasts, 2020–2027. 2020. Available online: https://www.reportlinker.com/p05930634/.html?utm_source=GNW (accessed on 8 January 2021).
3. Smirnov, A.A.; Selishcheva, S.A.; Yakovlev, V.A. Acetalization Catalysts for Synthesis of Valuable Oxygenated Fuel Additives from Glycerol. *Catalysts* **2018**, *8*, 595. [[CrossRef](#)]
4. Natalia, B.; Thomas, R.; Martin, K.; Stephan, A.S. Valorisation of Glycerol as Renewable Feedstock: Comparison of the Exploration of Chemical Transformation Methods Aided by High Throughput Experimentation. *Comb. Chem. High. Throughput Screen.* **2012**, *15*, 123–135. [[CrossRef](#)]
5. Rodrigues, A.; Bordado, J.C.; dos Santos, R.G. Upgrading the Glycerol from Biodiesel Production as a Source of Energy Carriers and Chemicals—A Technological Review for Three Chemical Pathways. *Energies* **2017**, *10*, 1817. [[CrossRef](#)]
6. Rahmat, N.; Abdullah, A.Z.; Mohamed, A.R. Recent progress on innovative and potential technologies for glycerol transformation into fuel additives: A critical review. *Renew. Sustain. Energy Rev.* **2010**, *14*, 987–1000. [[CrossRef](#)]
7. Checa, M.; Nogales-Delgado, S.; Montes, V.; Encinar, J.M. Recent Advances in Glycerol Catalytic Valorization: A Review. *Catalysts* **2020**, *10*, 1279. [[CrossRef](#)]
8. Kosamia, N.M.; Samavi, M.; Uprety, B.K.; Rakshit, S.K. Valorization of Biodiesel Byproduct Crude Glycerol for the Production of Bioenergy and Biochemicals. *Catalysts* **2020**, *10*, 609. [[CrossRef](#)]
9. Zhou, C.-H.; Beltramini, J.N.; Lin, C.-X.; Xu, Z.-P.; Lu, G.Q.; Tanksale, A. Selective oxidation of biorenewable glycerol with molecular oxygen over Cu-containing layered double hydroxide-based catalysts. *Catal. Sci. Technol.* **2011**, *1*, 111–122. [[CrossRef](#)]
10. Walgode, P.M.; Faria, R.P.V.; Rodrigues, A.E. A review of aerobic glycerol oxidation processes using heterogeneous catalysts: A sustainable pathway for the production of dihydroxyacetone. *Catal. Rev.* **2020**. [[CrossRef](#)]
11. Beltrán Prieto, J.C.; Kolomazník, K.; Pecha, J. A Review of Catalytic Systems for Glycerol Oxidation: Alternatives for Waste Valorization. *Aust. J. Chem.* **2013**, *66*, 511–521. [[CrossRef](#)]
12. Lari, G.M.; Mondelli, C.; Pérez-Ramírez, J. Gas-phase oxidation of glycerol to dihydroxyacetone over tailored iron zeolites. *ACS Catal.* **2015**, *5*, 1453–1461. [[CrossRef](#)]
13. Palacio, R.; Amaya, Á.A.; Blach, D.; Torres, S.; Hernández, D.; López, D.; Martínez, F. Influence of the Acid Properties of the Support on Au-Based Catalysts for Glycerol Oxidation in Aqueous Medium. *ChemistrySelect* **2020**, *5*, 7789–7796. [[CrossRef](#)]
14. Liu, L.; Ye, X.P.; Katryniok, B.; Capron, M.; Paul, S.; Dumeignil, F. Extending Catalyst Life in Glycerol-to-Acrolein Conversion Using Non-thermal Plasma. *Front. Chem.* **2019**. [[CrossRef](#)] [[PubMed](#)]
15. Dodekatos, G.; Abis, L.; Freakley, S.J.; Tüysüz, H.; Hutchings, G.J. Glycerol Oxidation Using MgO-and Al₂O₃-supported Gold and Gold–Palladium Nanoparticles Prepared in the Absence of Polymer Stabilizers. *ChemCatChem* **2018**, *10*, 1351–1359. [[CrossRef](#)]
16. Farnetti, E.; Crotti, C. Selective oxidation of glycerol to formic acid catalyzed by iron salts. *Catal. Commun.* **2016**, *84*, 1–4. [[CrossRef](#)]
17. Crotti, C.; Farnetti, E.J. Selective oxidation of glycerol catalyzed by iron complexes. *Mol. Catal. A Chem.* **2015**, *396*, 353–359. [[CrossRef](#)]
18. Xu, C.; Gan, J.; Mei, X.; Zhou, Y.; Duanmu, J.; Zhu, G.; Zhang, H.; Han, X.; Wang, Y.; Liu, S.-B. Highly Active Silver ion-Exchanged Silicotungstic Acid Catalysts for Selective Esterification of Glycerol with Lauric Acid. *Catal. Lett.* **2020**, *150*, 3584–3597. [[CrossRef](#)]
19. Narkhede, N.; Patel, A. Sustainable valorisation of glycerol via acetalization as well as carboxylation reactions over silicotungstates anchored to zeolite H β . *Appl. Catal. A Gen.* **2016**, *515*, 154–163. [[CrossRef](#)]
20. Florez-Rodriguez, P.P.; Pamphile-Adrián, A.J.; Passos, F.B. Glycerol conversion in the presence of carbon dioxide on alumina supported nickel catalyst. *Catal. Today* **2014**, *237*, 38–46. [[CrossRef](#)]
21. Barrault, J.; Jerome, F. Design of new solid catalysts for the selective conversion of glycerol. *Eur. J. Lipid Sci. Technol.* **2008**, *110*, 825–830. [[CrossRef](#)]
22. Oprescu, E.E.; Stepan, E.; Rosca, P.; Radu, A.; Enascuta, C. Synthesis of glycerol carbonate over hydrotalcite catalyst. *Rev. De Chim.* **2012**, *63*, 621–625.
23. Ruppert, A.M.; Meeldijk, J.D.; Kuipers, B.W.; Erné, B.H.; Weckhuysen, B.M. Glycerol etherification over highly active CaO-based materials: New mechanistic aspects and related colloidal particle formation. *Chem. (Weinh. Der Bergstr. Ger.)* **2008**, *14*, 2016–2024. [[CrossRef](#)] [[PubMed](#)]
24. Aguado-Deblas, L.; Estevez, R.; Russo, M.; La Parola, V.; Bautista, F.M.; Testa, M.L. Microwave-Assisted Glycerol Etherification Over Sulfonic Acid Catalysts. *Materials* **2020**, *13*, 1584. [[CrossRef](#)] [[PubMed](#)]
25. Guerrero-Urbaneja, P.; García-Sancho, C.; Moreno-Tost, R.; Mérida-Robles, J.; Santamaría-González, J.; Jiménez-López, A.; Maireles-Torres, P. Glycerol valorization by etherification to polyglycerols by using metal oxides derived from MgFe hydrotalcites. *Appl. Catal. A Gen.* **2014**, *470*, 199–207. [[CrossRef](#)]
26. Clacens, J.M.; Pouilloux, Y.; Barrault, J. Selective etherification of glycerol to polyglycerols over impregnated basic MCM-41 type mesoporous catalysts. *Appl. Catal. A Gen.* **2002**, *227*, 181–190. [[CrossRef](#)]
27. Magar, S.; Mohanraj, G.T.; Jana, S.K.; Rode, C.V. Synthesis and characterization of supported heteropoly acid: Efficient solid acid catalyst for glycerol esterification to produce biofuel additives. *Inorg. Nano-Met. Chem.* **2020**, *50*, 1157–1165. [[CrossRef](#)]

28. Reinoso, D.M.; Boldrini, D.E. Kinetic study of fuel bio-additive synthesis from glycerol esterification with acetic acid over acid polymeric resin as catalyst. *Fuel* **2020**, *264*, 116879. [[CrossRef](#)]
29. Aghbashlo, M.; Tabatabaei, M.; Rastegari, H.; Ghaziaskar, H.S.; Valijanian, E. Exergy-based optimization of a continuous reactor applied to produce value-added chemicals from glycerol through esterification with acetic acid. *Energy* **2018**, *150*, 351–362. [[CrossRef](#)]
30. Popova, M.; Lazarova, H.; Kalvachev, Y.; Todorova, T.; Szegedi, Á.; Shestakova, P.; Mali, G.; Dasireddy, V.D.B.C.; Likozar, B. Zr-modified hierarchical mordenite as heterogeneous catalyst for glycerol esterification. *Catal. Commun.* **2017**, *100*, 10–14. [[CrossRef](#)]
31. Gonzalez-Arellano, C.; Arancon, R.A.D.; Luque, R. Al-SBA-15 catalysed cross-esterification and acetalisation of biomass-derived platform chemicals. *Green Chem.* **2014**, *16*, 4985–4993. [[CrossRef](#)]
32. Gonzalez-Arellano, C.; De, S.; Luque, R. Selective glycerol transformations to high value-added products catalysed by aluminosilicate-supported iron oxide nanoparticles. *Catal. Sci. Technol.* **2014**, *4*, 4242–4249. [[CrossRef](#)]
33. Mallesham, B.; Sudarsanam, P.; Reddy, B.M. Production of Biofuel Additives from Esterification and Acetalization of Bioglycerol over SnO₂-Based Solid Acids. *Ind. Eng. Chem. Res.* **2014**, *53*, 18775–18785. [[CrossRef](#)]
34. Rastegari, H.; Ghaziaskar, H.S.; Yalpani, M. Valorization of Biodiesel Derived Glycerol to Acetins by Continuous Esterification in Acetic Acid: Focusing on High Selectivity to Diacetin and Triacetin with No Byproducts. *Ind. Eng. Chem. Res.* **2015**, *54*, 3279–3284. [[CrossRef](#)]
35. Mallesham, B.; Govinda Rao, B.; Reddy, B.M. Production of biofuel additives by esterification and acetalization of bioglycerol. *Comptes Rendus Chim.* **2016**, *19*, 1194–1202. [[CrossRef](#)]
36. Zhu, S.; Gao, X.; Dong, F.; Zhu, Y.; Zheng, H.; Li, Y. Design of a highly active silver-exchanged phosphotungstic acid catalyst for glycerol esterification with acetic acid. *J. Catal.* **2013**, *306*, 155–163. [[CrossRef](#)]
37. Gonzalez-Arellano, C.; Parra-Rodriguez, L.; Luque, R. Mesoporous Zr-SBA-16 catalysts for glycerol valorization processes: Towards biorenewable formulations. *Catal. Sci. Technol.* **2014**, *4*, 2287–2292. [[CrossRef](#)]
38. Okoye, P.U.; Wang, S.; Khanday, W.A.; Li, S.; Tang, T.; Zhang, L. Box-Behnken optimization of glycerol transesterification reaction to glycerol carbonate over calcined oil palm fuel ash derived catalyst. *Renew. Energy* **2020**, *146*, 2676–2687. [[CrossRef](#)]
39. Devarajan, A.; Thiripuranthagan, S.; Radhakrishnan, R.; Kumaravel, S. Solvent Free Transesterification of Glycerol Into Glycerol Carbonate Over Nanostructured CaAl Hydrotalcite Catalyst. *J. Nanosci. Nanotechnol.* **2018**, *18*, 4588–4599. [[CrossRef](#)]
40. Shafiei, A.; Rastegari, H.; Ghaziaskar, H.S.; Yalpani, M. Glycerol transesterification with ethyl acetate to synthesize acetins using ethyl acetate as reactant and entrainer. *Biofuel Res. J.* **2017**, *4*, 565–570. [[CrossRef](#)]
41. Morales, G.; Paniagua, M.; Melero, J.A.; Vicente, G.; Ochoa, C. Sulfonic Acid-Functionalized Catalysts for the Valorization of Glycerol via Transesterification with Methyl Acetate. *Ind. Eng. Chem. Res.* **2011**, *50*, 5898–5906. [[CrossRef](#)]
42. Simón, D.; Borreguero, A.M.; de Lucas, A.; Rodríguez, J.F. Valorization of crude glycerol as a novel transesterification agent in the glycolysis of polyurethane foam waste. *Polym. Degrad. Stab.* **2015**, *121*, 126–136. [[CrossRef](#)]
43. Esteban, J.; Domínguez, E.; Ladero, M.; Garcia-Ochoa, F. Kinetics of the production of glycerol carbonate by transesterification of glycerol with dimethyl and ethylene carbonate using potassium methoxide, a highly active catalyst. *Fuel Process. Technol.* **2015**, *138*, 243–251. [[CrossRef](#)]
44. Tavor, D.; Sheviev, O.; Dlugy, C.; Wolfson, A. Transfer hydrogenations of benzaldehyde using glycerol as solvent and hydrogen source. *Can. J. Chem.* **2010**, *88*, 305–308. [[CrossRef](#)]
45. Crabtree, R.H. Transfer Hydrogenation with Glycerol as H-Donor: Catalyst Activation, Deactivation and Homogeneity. *ACS Sustain. Chem. Eng.* **2019**, *7*, 15845–15853. [[CrossRef](#)]
46. Crotti, C.; Kašpar, J.; Farnetti, E. Dehydrogenation of glycerol to dihydroxyacetone catalyzed by iridium complexes with P–N ligands. *Green Chem.* **2010**, *12*, 1295–1300. [[CrossRef](#)]
47. Farnetti, E.; Kašpar, J.; Crotti, C. A novel glycerol valorization route: Chemoselective dehydrogenation catalyzed by iridium derivatives. *Green Chem.* **2009**, *11*, 704–709. [[CrossRef](#)]
48. Dusescu, C.; Bolocan, I. New catalysts for the glycerol hydrogenolysis. *Rev. De Chim.* **2012**, *63*, 732–738.
49. Liang, Y.; Shi, G.; Jin, K. Promotion Effect of Al₂O₃ on Pt–WO_x/SiO₂ Catalysts for Selective Hydrogenolysis of Bioglycerol to 1,3-Propanediol in Liquid Phase. *Catal. Lett.* **2020**, *150*, 2365–2376. [[CrossRef](#)]
50. Lei, N.; Zhao, X.; Hou, B.; Yang, M.; Zhou, M.; Liu, F.; Wang, A.; Zhang, T. Effective Hydrogenolysis of Glycerol to 1,3-Propanediol over Metal-Acid Concerted Pt/WO_x/Al₂O₃ Catalysts. *ChemCatChem* **2019**, *11*, 3903–3912. [[CrossRef](#)]
51. Von Held Soares, A.; Atia, H.; Armbruster, U.; Passos, F.B.; Martin, A. Platinum, palladium and nickel supported on Fe₃O₄ as catalysts for glycerol aqueous-phase hydrogenolysis and reforming. *Appl. Catal. A Gen.* **2017**, *548*, 179–190. [[CrossRef](#)]
52. Mallesham, B.; Sudarsanam, P.; Reddy, B.V.S.; Reddy, B.M. Development of cerium promoted copper–magnesium catalysts for biomass valorization: Selective hydrogenolysis of bioglycerol. *Appl. Catal. B Environ.* **2016**, *181*, 47–57. [[CrossRef](#)]
53. Mauriello, F.; Ariga, H.; Musolino, M.G.; Pietropaolo, R.; Takakusagi, S.; Asakura, K. Exploring the catalytic properties of supported palladium catalysts in the transfer hydrogenolysis of glycerol. *Appl. Catal. B Environ.* **2015**, *166*, 121–131. [[CrossRef](#)]
54. Lari, G.M.; García-Muelas, R.; Mondelli, C.; López, N.; Pérez-Ramírez, J. Glycerol oxidehydration to pyruvaldehyde over silver-based catalysts for improved lactic acid production. *Green Chem.* **2016**, *18*, 4682–4692. [[CrossRef](#)]
55. Liu, L.; Wang, B.; Du, Y.; Borgna, A. Supported H₄SiW₁₂O₄₀/Al₂O₃ solid acid catalysts for dehydration of glycerol to acrolein: Evolution of catalyst structure and performance with calcination temperature. *Appl. Catal. A Gen.* **2015**, *489*, 32–41. [[CrossRef](#)]

56. Rao, G.S.; Rajan, N.P.; Pavankumar, V.; Chary, K.V.R. Vapour phase dehydration of glycerol to acrolein over NbOPO₄ catalysts. *J. Chem. Technol. Biotechnol.* **2014**, *89*, 1890–1897. [[CrossRef](#)]
57. Yadav, G.D.; Sharma, R.V.; Katole, S.O. Selective Dehydration of Glycerol to Acrolein: Development of Efficient and Robust Solid Acid Catalyst MUICaT-5. *Ind. Eng. Chem. Res.* **2013**, *52*, 10133–10144. [[CrossRef](#)]
58. Shiju, N.R.; Brown, D.R.; Wilson, K.; Rothenberg, G. Glycerol Valorization: Dehydration to Acrolein Over Silica-Supported Niobia Catalysts. *Top. Catal.* **2010**, *53*, 1217–1223. [[CrossRef](#)]
59. Katryniok, B.; Paul, S.; Capron, M.; Dumeignil, F. Towards the sustainable production of acrolein by glycerol dehydration. *ChemSusChem* **2009**, *2*, 719–730. [[CrossRef](#)]
60. Caputo, D.; Casiello, M.; Milella, A.; Oberhauser, W.; Maffezzoli, A.; Nacci, A.; Fusco, C.; D'Accolti, L. Deep Control of Linear Oligomerization of Glycerol Using Lanthanum Catalyst on Mesoporous Silica Gel. *Catalysts* **2020**, *10*, 1170. [[CrossRef](#)]
61. Zandoni, A.; Gardoni, G.; Sponchioni, M.; Moscatelli, D. Valorisation of glycerol and CO₂ to produce biodegradable polymer nanoparticles with a high percentage of bio-based components. *J. CO₂ Util.* **2020**, *40*, 101192. [[CrossRef](#)]
62. Barros, F.J.S.; Cecilia, J.A.; Moreno-Tost, R.; de Oliveira, M.F.; Rodríguez-Castellón, E.; Luna, F.M.T.; Vieira, R.S. Glycerol Oligomerization Using Low Cost Dolomite Catalyst. *Waste Biomass Valorization* **2020**, *11*, 1499–1512. [[CrossRef](#)]
63. Pham, P.D.; Monge, S.; Lapinte, V.; Raoul, Y.; Robin, J.J. Glycerol-based co-oligomers by free-radical chain transfer polymerization: Towards reactive polymers bearing acetal and/or carbonate groups with enhanced properties. *Eur. Polym. J.* **2017**, *95*, 491–502. [[CrossRef](#)]
64. Barrault, J.; Clacens, J.M.; Pouilloux, Y. Selective Oligomerization of Glycerol Over Mesoporous Catalysts. *Top. Catal.* **2004**, *27*, 137–142. [[CrossRef](#)]
65. Zhang, H.; Li, H.; Wang, A.; Xu, C.; Yang, S. Progress of Catalytic Valorization of Bio-Glycerol with Urea into Glycerol Carbonate as a Monomer for Polymeric Materials. *Adv. Polym. Technol.* **2020**, *2020*, 7207068. [[CrossRef](#)]
66. Jang, H.-S.; Bae, K.; Shin, M.; Kim, S.M.; Kim, C.-U.; Suh, Y.-W. Aromatization of glycerol/alcohol mixtures over zeolite H-ZSM-5. *Fuel* **2014**, *134*, 439–447. [[CrossRef](#)]
67. Torres, D.; Arcelus-Arrillaga, P.; Millan, M.; Pinilla, J.L.; Suelves, I. Enhanced Reduction of Few-Layer Graphene Oxide via Supercritical Water Gasification of Glycerol. *Nanomaterials* **2017**, *7*, 447. [[CrossRef](#)]
68. Almeida, A.; Ribeiro, A.; Ramalho, E.; Pilão, R. Crude glycerol gasification in a fixed bed gasifier. *Energy Procedia* **2018**, *153*, 149–153. [[CrossRef](#)]
69. Charisiou, N.D.; Siakavelas, G.I.; Papageridis, K.N.; Motta, D.; Dimitratos, N.; Sebastian, V.; Polychronopoulou, K.; Goula, M.A. The Effect of Noble Metal (M: Ir, Pt, Pd) on M/Ce₂O₃-γ-Al₂O₃ Catalysts for Hydrogen Production via the Steam Reforming of Glycerol. *Catalysts* **2020**, *10*, 790. [[CrossRef](#)]
70. Bac, S.; Keskin, S.; Avci, A.K. Recent advances in sustainable syngas production by catalytic CO₂ reforming of ethanol and glycerol. *Sustain. Energy Fuels* **2020**, *4*, 1029–1047. [[CrossRef](#)]
71. Remón, J.; Jarauta-Córdoba, C.; García, L.; Arauzo, J. Effect of acid (CH₃COOH, H₂SO₄ and H₃PO₄) and basic (KOH and NaOH) impurities on glycerol valorisation by aqueous phase reforming. *Appl. Catal. B Environ.* **2017**, *219*, 362–371. [[CrossRef](#)]
72. Esteve-Adell, I.; Crapart, B.; Primo, A.; Serp, P.; Garcia, H. Aqueous phase reforming of glycerol using doped graphenes as metal-free catalysts. *Green Chem.* **2017**, *19*, 3061–3068. [[CrossRef](#)]
73. Remón, J.; Giménez, J.R.; Valiente, A.; García, L.; Arauzo, J. Production of gaseous and liquid chemicals by aqueous phase reforming of crude glycerol: Influence of operating conditions on the process. *Energy Convers. Manag.* **2016**, *110*, 90–112. [[CrossRef](#)]
74. Iliuta, I.; Iliuta, M.C. Integration of sorption-enhanced steam glycerol reforming with methanation of in-situ removed carbon dioxide—An alternative for glycerol valorization. *Int. J. Hydrog. Energy* **2020**, *45*, 18574–18586. [[CrossRef](#)]
75. Roslan, N.A.; Abidin, S.Z.; Ideris, A.; Vo, D.-V.N. A review on glycerol reforming processes over Ni-based catalyst for hydrogen and syngas productions. *Int. J. Hydrog. Energy* **2020**, *45*, 18466–18489. [[CrossRef](#)]
76. Lin, Y.-C. Catalytic valorization of glycerol to hydrogen and syngas. *Int. J. Hydrog. Energy* **2013**, *38*, 2678–2700. [[CrossRef](#)]
77. Dodson, J.R.; Avellar, T.; Athayde, J.; Mota, C.J.A. Glycerol acetals with antioxidant properties. *Pure Appl. Chem.* **2014**, *86*, 905–911. [[CrossRef](#)]
78. Malleshham, B.; Sudarsanam, P.; Reddy, B.M. Eco-friendly synthesis of bio-additive fuels from renewable glycerol using nanocrystalline SnO₂-based solid acids. *Catal. Sci. Technol.* **2014**, *4*, 803–813. [[CrossRef](#)]
79. Deutsch, J.; Martin, A.; Lieske, H. Investigations on heterogeneously catalysed condensations of glycerol to cyclic acetals. *J. Catal.* **2007**, *245*, 428–435. [[CrossRef](#)]
80. Leng, Y.; Zhao, J.; Jiang, P.; Lu, D. POSS-derived solid acid catalysts with excellent hydrophobicity for highly efficient transformations of glycerol. *Catal. Sci. Technol.* **2016**, *6*, 875–881. [[CrossRef](#)]
81. Malleshham, B.; Sudarsanam, P.; Raju, G.; Reddy, B.M. Design of highly efficient Mo and W-promoted SnO₂ solid acids for heterogeneous catalysis: Acetalization of bio-glycerol. *Green Chem.* **2013**, *15*, 478–489. [[CrossRef](#)]
82. Manjunathan, P.; Marakatti, V.S.; Chandra, P.; Kulal, A.B.; Umbarkar, S.B.; Ravishankar, R.; Shanbhag, G.V. Mesoporous tin oxide: An efficient catalyst with versatile applications in acid and oxidation catalysis. *Catal. Today* **2018**, *309*, 61–76. [[CrossRef](#)]
83. Udayakumar, V.; Pandurangan, A. Synthesis of Hf/SBA-15 Lewis acid catalyst for converting glycerol to value-added chemicals. *J. Porous Mater.* **2017**, *24*, 979–990. [[CrossRef](#)]

84. Kundu, S.K.; Singuru, R.; Hayashi, T.; Hijikata, Y.; Irle, S.; Mondal, J. Constructing Sulfonic Acid Functionalized Anthracene Derived Conjugated Porous Organic Polymer for Efficient Metal-Free Catalytic Acetalization of Bio-Glycerol. *ChemistrySelect* **2017**, *2*, 4705–4716. [[CrossRef](#)]
85. Poly, S.S.; Jamil, M.A.R.; Touchy, A.S.; Yasumura, S.; Siddiki, S.M.A.H.; Toyao, T.; Maeno, Z.; Shimizu, K.-I. Acetalization of glycerol with ketones and aldehydes catalyzed by high silica H β zeolite. *Mol. Catal.* **2019**, *479*, 110608. [[CrossRef](#)]
86. Pawar, R.R.; Gosai, K.A.; Bhatt, A.S.; Kumaresan, S.; Lee, S.M.; Bajaj, H.C. Clay catalysed rapid valorization of glycerol towards cyclic acetals and ketals. *RSC Adv.* **2015**, *5*, 83985–83996. [[CrossRef](#)]
87. Elena-Emilia, O.; Bombos, D.; Bolocan, I.; Dragomir, R.; Rosca, P. Diesel Fuel Green Additive based on Glycerol. *Rev. De Chim. Buchar. Orig. Ed.* **2014**, *65*, 1226–1229.
88. Narkhede, N.; Patel, A. Room temperature acetalization of glycerol to cyclic acetals over anchored silicotungstates under solvent free conditions. *RSC Adv.* **2014**, *4*, 19294–19301. [[CrossRef](#)]
89. Faria, R.P.V.; Pereira, C.S.M.; Silva, V.M.T.M.; Loureiro, J.M.; Rodrigues, A.E. Glycerol Valorization as Biofuel: Thermodynamic and Kinetic Study of the Acetalization of Glycerol with Acetaldehyde. *Ind. Eng. Chem. Res.* **2013**, *52*, 1538–1547. [[CrossRef](#)]
90. Crotti, C.; Farnetti, E.; Guidolin, N. Alternative intermediates for glycerol valorization: Iridium-catalyzed formation of acetals and ketals. *Green Chem.* **2010**, *12*, 2225–2231. [[CrossRef](#)]
91. Ruiz, V.R.; Velty, A.; Santos, L.L.; Leyva-Pérez, A.; Sabater, M.J.; Iborra, S.; Corma, A. Gold catalysts and solid catalysts for biomass transformations: Valorization of glycerol and glycerol–water mixtures through formation of cyclic acetals. *J. Catal.* **2010**, *271*, 351–357. [[CrossRef](#)]
92. Han, X.; Yan, W.; Chen, K.; Hung, C.-T.; Liu, L.-L.; Wu, P.-H.; Huang, S.-J.; Liu, S.-B. Heteropolyacid-based ionic liquids as effective catalysts for the synthesis of benzaldehyde glycol acetal. *Appl. Catal. A Gen.* **2014**, *485*, 149–156.
93. Umbarkar, S.B.; Kotbagi, T.V.; Biradar, A.V.; Pasricha, R.; Chanale, J.; Dongare, M.K.; Mamede, A.-S.; Lancelot, C.; Payen, E.J. Acetalization of glycerol using mesoporous MoO $_3$ /SiO $_2$ solid acid catalyst. *Mol. Catal. A Chem.* **2009**, *310*, 150–158. [[CrossRef](#)]
94. Talebian-Kiakalaieh, A.; Amin, N.A.S.; Najaafi, N.; Tarighi, S. A Review on the Catalytic Acetalization of Bio-renewable Glycerol to Fuel Additives. *Front. Chem.* **2018**, *6*, 573. [[CrossRef](#)] [[PubMed](#)]
95. Yip, L.; Kubczyk, T.M.; Davies, T.E.; Taylor, S.H.; Apperley, D.C.; Graham, A.E. Nanoporous aluminosilicate mediated transacetalization reactions: Application in glycerol valorization. *Catal. Sci. Technol.* **2012**, *2*, 2258–2263. [[CrossRef](#)]
96. Nanda, M.R.; Zhang, Y.; Yuan, Z.; Qin, W.; Ghaziaskar, H.S.; Xu, C. Catalytic conversion of glycerol for sustainable production of solketal as a fuel additive: A review. *Renew. Sust. Energ. Rev.* **2016**, *56*, 1022–1031. [[CrossRef](#)]
97. Moity, L.; Benazzouz, A.; Molinier, V.; Nardello-Rataj, V.; Elmaddem, M.K.; de Caro, P.; Thiébaud-Roux, S.; Gerbaud, V.; Marion, P.; Aubry, J.-M. Glycerol acetals and ketals as bio-based solvents: Positioning in Hansen and COSMO-RS spaces, volatility and stability towards hydrolysis and autoxidation. *Green Chem.* **2015**, *17*, 1779–1792. [[CrossRef](#)]
98. Stepan, E.; Enascuta, C.-E.; Oprescu, E.-E.; Radu, E.; Vasilievici, G.; Radu, A.; Stoica, R.; Velea, S.; Nicolescu, A.; Lavric, V. A versatile method for obtaining new oxygenated fuel components from biomass. *Ind. Crop. Prod.* **2018**, *113*, 288–297. [[CrossRef](#)]
99. Wegenhart, B.L.; Abu-Omar, M.M. A Solvent-Free Method for Making Dioxolane and Dioxane from the Biorenewables Glycerol and Furfural Catalyzed by Oxorhenium(V) Oxazoline. *Inorg. Chem.* **2010**, *49*, 4741–4743. [[CrossRef](#)]
100. Climent, M.J.; Corma, A.; Velty, A. Synthesis of hyacinth, vanilla, and blossom orange fragrances: The benefit of using zeolites and delaminated zeolites as catalysts. *Appl. Catal. A Gen.* **2004**, *263*, 155–161. [[CrossRef](#)]
101. Gutiérrez-Acebo, E.; Guerrero-Ruiz, F.; Centenero, M.; Martínez, J.S.; Salagre, P.; Cesteros, Y. Effect of using microwaves for catalysts preparation on the catalytic acetalization of glycerol with furfural to obtain fuel additives. *Open Chem.* **2018**, *16*, 386–392.
102. Adam, F.; Hassan, H.E.; Hello, K.M. The synthesis of N-heterocyclic carbene–silica nano-particles and its catalytic activity in the cyclization of glycerol. *J. Taiwan Inst. Chem. E.* **2012**, *43*, 619–630. [[CrossRef](#)]
103. Konwar, L.J.; Samikannu, A.; Mäki-Arvela, P.; Boström, D.; Mikkola, J.-P. Lignosulfonate-based macro/mesoporous solid protonic acids for acetalization of glycerol to bio-additives. *Appl. Catal. B Environ.* **2018**, *220*, 314–323. [[CrossRef](#)]
104. Zeitsch, K.J. *The Chemistry and Technology of Furfural and Its Many by-Products*, 13th ed; Sugar Series; Elsevier: Amsterdam, The Netherlands, 2000.
105. Vasiliou, A.K.; Kim, J.H.; Ormond, T.K.; Piech, K.M.; Urness, K.N.; Scheer, A.M.; Robichaud, D.J.; Mukarakate, C.; Nimlos, M.R.; Daily, J.W.; et al. Biomass pyrolysis: Thermal decomposition mechanisms of furfural and benzaldehyde. *J. Chem. Phys.* **2013**, *139*, 104310. [[CrossRef](#)] [[PubMed](#)]
106. Patil, A.; Shinde, S.; Kamble, S.; Rode, C.V. Two-Step Sequence of Acetalization and Hydrogenation for Synthesis of Diesel Fuel Additives from Furfural and Diols. *Energy Fuels* **2019**, *33*, 7466–7472. [[CrossRef](#)]
107. Pawar, R.R.; Jadhav, S.V.; Bajaj, H.C. Microwave-assisted rapid valorization of glycerol towards acetals and ketals. *Chem. Eng. J.* **2014**, *235*, 61–66.
108. Ferreira, G.K.B.; Carvalho, C.; Nakagaki, S. Studies of the Catalytic Activity of Iron (III) Porphyrins for the Protection of Carbonyl Groups in Homogeneous Media. *Catalysts* **2019**, *9*, 334. [[CrossRef](#)]
109. Wang, B.; Shen, Y.; Sun, J.; Xu, F.; Sun, R. Conversion of platform chemical glycerol to cyclic acetals promoted by acidic ionic liquids. *RSC Adv.* **2014**, *4*, 18917–18923. [[CrossRef](#)]
110. Yamamoto, K.; Kiyari, A.M.; Bagio, J.C.; Rossi, K.A.B.; Berezuk, F.D.; Berezuk, M.E. Green cyclic acetals production by glycerol etherification reaction with benzaldehyde using cationic acidic resin. *Green Process. Synth.* **2019**, *8*, 183–190. [[CrossRef](#)]

111. Sudarsanam, P.; Malleshham, B.; Prasad, A.N.; Reddy, P.S.; Reddy, B.M. Synthesis of bio-additive fuels from acetalization of glycerol with benzaldehyde over molybdenum promoted green solid acid catalysts. *Fuel Process. Technol.* **2013**, *106*, 539–545. [CrossRef]
112. Adam, F.; Batagarawa, M.S.; Hello, K.M.; Al-Juaid, S.S. One-step synthesis of solid sulfonic acid catalyst and its application in the acetalization of glycerol: Crystal structure of cis-5-hydroxy-2-phenyl-1,3-dioxane trimer. *Chem. Pap.* **2012**, *66*, 1048–1058.
113. Patel, A.; Pithadia, D. Low temperature synthesis of bio-fuel additives via valorisation of glycerol with benzaldehyde as well as furfural over a novel sustainable catalyst, 12-tungstosilicic acid anchored to ordered cubic nano-porous MCM-48. *Appl. Catal. A Gen.* **2020**, *602*, 117729. [CrossRef]
114. Wegenhart, B.L.; Liu, S.; Thom, M.; Stanley, D.; Abu-Omar, M.M. Solvent-Free Methods for Making Acetals Derived from Glycerol and Furfural and Their Use as a Biodiesel Fuel Component. *ACS Catal.* **2012**, *2*, 2524–2530. [CrossRef]
115. Bombos, D.; Velea, S.; Bombos, M.; Vasilevici, G.; Oprescu, E. Ecological Component for Motor Fuels Based on Furfural Derivates. *Rev. Chim-Bucharest* **2016**, *67*, 745–750.
116. Mendes, R.F.; Antunes, M.M.; Silva, P.; Barbosa, P.; Figueiredo, F.; Linden, A.; Rocha, J.; Valente, A.A.; Paz, F.A.A. A Lamellar Coordination Polymer with Remarkable Catalytic Activity. *Chem. Eur. J.* **2016**, *22*, 13136–13146. [CrossRef] [PubMed]
117. Mirante, F.; Mendes, R.M.; Paz, F.A.A.; Balula, S.S. High Catalytic Efficiency of a Layered Coordination Polymer to Remove Simultaneous Sulfur and Nitrogen Compounds from Fuels. *Catalysts* **2020**, *10*, 731. [CrossRef]
118. Win, D.T. Furfural—Gold from Garbage. *Au J. Technol.* **2005**, *8*, 185–190.
119. Mamman, A.S.; Lee, J.-M.; Kim, Y.-C.; Hwang, I.T.; Park, N.-J.; Hwang, Y.K.; Chang, J.-S.; Hwang, J.-S. Furfural: Hemicellulose/xylo-derived biochemical. *Biofuel Bioprod. Bior.* **2008**, *2*, 438–454.
120. Research and Markets, Furfural and Furfuryl Alcohol: A Global Market Overview. 2018. Available online: <https://www.researchandmarkets.com/reports/4622226/furfural-and-furfuryl-alcohol-a-global-market> (accessed on 9 January 2021).
121. Maldonado, G.M.G.; Assary, R.S.; Dumesic, J.A.; Curtiss, L.A. Acid-catalyzed conversion of furfuryl alcohol to ethyl levulinate in liquid ethanol. *Energy Environ. Sci.* **2012**, *5*, 8990–8997. [CrossRef] [PubMed]
122. Eerhart, A.J.J.E.; Patel, M.K.; Faaij, A.P.C. Fuels and plastics from lignocellulosic biomass via the furan pathway: An economic analysis. *Biofuel Bioprod. Bior.* **2015**, *9*, 307–325. [CrossRef]
123. Haan, R.J.; Lange, J.-P. Gasoline Composition and Process for the Preparation of Alkylfurfuryl ether. U.S. Patent 8,372,164 B2, 12 February 2013. Available online: <https://patentimages.storage.googleapis.com/c2/6f/90/cc012182280cd3/US8372164.pdf> (accessed on 9 January 2021).
124. Haan, J.R.; Lange, J.-P. Gasoline Composition and Process for the Preparation of Alkylfurfuryl ether. International Application Number: PCT/EP2008/067937. WO 2009/077606 A2, 25 June 2009. Available online: <https://patentimages.storage.googleapis.com/7d/5d/a9/23f35e898d5267/WO2009077606A2.pdf> (accessed on 9 January 2021).
125. Bhansali, K.J.; Bhagat, P.R. Perylene supported metal free brønsted acid-functionalized porphyrin intertwined with benzimidazolium moiety for enhanced photocatalytic etherification of furfuryl alcohol. *Fuel* **2020**, *278*, 118394. [CrossRef]
126. Paniagua, M.; Melero, J.A.; Iglesias, J.; Morales, G.; Hernández, B.; López-Aguado, C. Catalytic upgrading of furfuryl alcohol to bio-products: Catalysts screening and kinetic analysis. *Appl. Catal. A Gen.* **2017**, *537*, 74–82. [CrossRef]
127. Vanderhaegen, B.; Neven, H.; Daenen, L.; Verstrepen, K.J.; Verachtert, H.; Derdelinckx, G.J. Furfuryl ethyl ether: Important aging flavor and a new marker for the storage conditions of beer. *Agr. Food Chem.* **2004**, *52*, 1661–1668. [CrossRef]
128. Vanderhaegen, B.; Neven, H.; Coghe, S.; Verstrepen, K.J.; Verachtert, H.; Derdelinckx, G. Evolution of Chemical and Sensory Properties during Aging of Top-Fermented Beer. *J. Agr. Food Chem.* **2003**, *51*, 6782–6790. [CrossRef]
129. Vanderhaegen, B.; Neven, H.; Verstrepen, K.J.; Delvaux, F.R.; Verachtert, H.; Derdelinckx, G.J. Influence of the Brewing Process on Furfuryl Ethyl Ether Formation during Beer Aging. *Agr. Food Chem.* **2004**, *52*, 6755–6764. [CrossRef]
130. Herrmann, M.; Klotzbücher, B.; Wurzbacher, M.; Hanke, S.; Kattein, U.; Back, W.; Becker, T.; Krottenthaler, M.J.I. A New Validation of Relevant Substances for the Evaluation of Beer Aging Depending on the Employed Boiling System. *Brewing* **2010**, *116*, 41–48. [CrossRef]
131. Harayama, K.; Hayase, F.; Kato, H. Contribution to Stale Flavor of 2-Furfuryl Ethyl Ether and Its Formation Mechanism in Beer. *Biosci. Biotech. Bioch.* **1995**, *59*, 1144–1146. [CrossRef]
132. Spillman, P.J.; Pollnitz, A.P.; Liacopoulos, D.; Pardon, K.H.; Sefton, M.A. Formation and Degradation of Furfuryl Alcohol, 5-Methylfurfuryl Alcohol, Vanillyl Alcohol, and Their Ethyl Ethers in Barrel-Aged Wines. *J. Agr. Food Chem.* **1998**, *46*, 657–663. [CrossRef] [PubMed]
133. Johannes, G.; Gruter, M. S-substituted 2-(alkoxymethyl)furans. U.S. Patent 8,231,693 B2, 31 July 2012. Available online: <https://patentimages.storage.googleapis.com/43/72/8d/7aa4856861283b/US8231693.pdf> (accessed on 9 January 2021).
134. Patil, C.R.; Rode, C.V. Selective Production of Furanic Ethers from Lignocellulosic Biomass over Mesoporous Zr-Incorporated SBA-15 Catalyst. *ChemistrySelect* **2018**, *3*, 12504–12511.
135. Eerhart, A.J.J.E.; Huijgen, W.J.J.; Grisel, R.J.H.; van der Waal, J.C.; de Jong, E.; de Dias, A.S.; Faaij, A.P.C.; Patel, M.K. Fuels and plastics from lignocellulosic biomass via the furan pathway; a technical analysis. *RSC Adv.* **2014**, *4*, 3536–3549. [CrossRef]
136. Mulik, N.L.; Niphadkar, P.S.; Bokade, V. Synthesis of ethyl furfuryl ether (potential biofuel) by etherification of furfuryl alcohol with ethanol over heterogenized reusable H1Cs2PW₁₂O₄₀ catalyst. *Res. Chem. Intermediat.* **2020**, *46*, 2309–2325. [CrossRef]
137. Chaffey, D.R.; Davies, T.E.; Taylor, S.H.; Graham, A.E. Etherification Reactions of Furfuryl Alcohol in the Presence of Orthoesters and Ketals: Application to the Synthesis of Furfuryl Ether Biofuels. *ACS Sustain. Chem. Eng.* **2018**, *6*, 4996–5002. [CrossRef]

138. Hu, D.; Hu, H.; Jin, H.; Zhang, P.; Hu, Y.; Ying, S.; Li, X.; Yang, Y.; Zhang, J.; Wang, L. Building hierarchical zeolite structure by post-synthesis treatment to promote the conversion of furanic molecules into biofuels. *Appl. Catal. A Gen.* **2020**, *590*, 117338. [CrossRef]
139. Tian, M.; McCormick, R.L.; Luecke, J.; de Jong, E.; van der Waal, J.C.; van Klink, G.P.M.; Boot, M.D. Anti-knock quality of sugar derived levulinic esters and cyclic ether. *Fuel* **2017**, *202*, 414–425. [CrossRef]
140. De Jong, E.; Vijlbrief, T.; Hijkoop, R.; Gruter, J.-G.M.; van der Waal, J.C. Promising results with YXY Diesel components in an ESC test cycle using a PACCAR Diesel engine. *Biomass Bioenerg.* **2012**, *36*, 151–159. [CrossRef]
141. Silva, J.F.L.; Grekin, R.; Mariano, A.P.; Filho, R.M. Making Levulinic Acid and Ethyl Levulinate Economically Viable: A Worldwide Technoeconomic and Environmental Assessment of Possible Routes. *Energy Technol. Ger.* **2018**, *6*, 613–639. [CrossRef]
142. Ahmad, E.; Alam, M.I.; Pant, K.K.; Haider, M.A. Catalytic and mechanistic insights into the production of ethyl levulinate from biorenewable feedstocks. *Green Chem.* **2016**, *18*, 4804–4823. [CrossRef]
143. Grand View Research, Ethyl Levulinate Market Size, Share and Trends Analysis Report by Application (Flavors, Fragrance), by Region (North America, Europe, Asia Pacific, Middle East and Africa, Central and South America) and Segment Forecast, 2015–2022. 2016. Available online: <https://www.grandviewresearch.com/industry-analysis/ethyl-levulinate-market> (accessed on 9 January 2021).
144. Lange, J.-P.; van der Heide, E.; van Buijtenen, J.; Price, R. Furfural—A Promising Platform for Lignocellulosic Biofuels. *ChemSusChem* **2012**, *5*, 150–166. [CrossRef]
145. Gupta, S.S.R.; Kantam, M.L. Catalytic conversion of furfuryl alcohol or levulinic acid into alkyl levulinates using a sulfonic acid-functionalized hafnium-based MOF. *Catal. Commun.* **2019**, *124*, 62–66. [CrossRef]
146. Liu, X.; Pan, H.; Zhang, H.; Li, H.; Yang, S. Efficient Catalytic Upgradation of Bio-Based Furfuryl Alcohol to Ethyl Levulinate Using Mesoporous Acidic MIL-101(Cr). *ACS Omega* **2019**, *4*, 8390–8399. [CrossRef] [PubMed]
147. Liu, X.-F.; Li, H.; Zhang, H.; Pan, H.; Huang, S.; Yang, K.-L.; Yang, S. Efficient conversion of furfuryl alcohol to ethyl levulinate with sulfonic acid-functionalized MIL-101(Cr). *RSC Adv.* **2016**, *6*, 90232–90238. [CrossRef]
148. Kolb, M.; Wichmann, H.; Schröder, U. GC/MS-screening analyses of valuable products in the aqueous phase from microwave-assisted hydrothermal processing of Lemna minor. *Sustain. Chem. Pharm.* **2019**, *13*, 100165. [CrossRef]
149. Vermeire, F.H.; Carstensen, H.-H.; Herbinet, O.; Battin-Leclerc, F.; Marin, G.B.; Van Geem, K.M. The thermal decomposition of furfural: Molecular chemistry unraveled. *P. Combust. Inst.* **2019**, *37*, 445–452. [CrossRef]
150. Furfuryl Alcohol Market Size, Share & Trends Analysis Report By Application (Resins, Solvent, Corrosion Inhibitor), By End Use (Foundry, Agriculture), By Region, And Segment Forecasts, 2020–2027. 2020. Available online: <https://www.grandviewresearch.com/industry-analysis/furfuryl-alcohol-market> (accessed on 9 January 2021).
151. Tiong, Y.W.; Yap, C.L.; Gan, S.; Yap, W.S.P. Conversion of Biomass and Its Derivatives to Levulinic Acid and Levulinate Esters via Ionic Liquids. *Ind. Eng. Chem. Res.* **2018**, *57*, 4749–4766. [CrossRef]
152. Kołodziejka, D.; Gęca, M.; Siek, M.; Hubicki, Z. Nitritotris(methylenephosphonic) acid as a complexing agent in sorption of heavy metal ions on ion exchangers. *Chem. Eng. J.* **2013**, *215*, 948–958. [CrossRef]
153. Vilela, S.M.F.; Ananias, D.; Fernandes, J.A.; Silva, P.; Gomes, A.C.; Silva, N.J.O.; Rodrigues, M.O.; Tomé, J.P.C.; Valente, A.A.; Ribeiro-Claro, P.; et al. Multifunctional micro- and nanosized metal-organic frameworks assembled from bisphosphonates and lanthanides. *J. Mater. Chem. C* **2014**, *2*, 3311–3327. [CrossRef]
154. Monteiro, B.; Fernandes, J.A.; Pereira, C.C.L.; Vilela, S.M.F.; Tome, J.P.C.; Marcalo, J.; Paz, F.A.A. Metal-organic frameworks based on uranyl and phosphonate ligands. *Acta Crystallogr. B* **2014**, *70*, 28–36. [CrossRef] [PubMed]
155. Nanda, M.R.; Yuan, Z.; Qin, W.; Ghaziaskar, H.S.; Poirier, M.-A.; Xu, C.C. Thermodynamic and kinetic studies of a catalytic process to convert glycerol into solketal as an oxygenated fuel additive. *Fuel* **2014**, *117*, 470–477. [CrossRef]
156. Song, D.; An, S.; Sun, Y.; Guo, Y. Efficient conversion of levulinic acid or furfuryl alcohol into alkyl levulinates catalyzed by heteropoly acid and ZrO₂ bifunctionalized organosilica nanotubes. *J. Catal.* **2016**, *333*, 184–199. [CrossRef]
157. Guo, H.; Abe, Y.; Qi, X.; Smith, R.L., Jr. Bifunctional carbon Ni/NiO nanofiber catalyst based on 5-sulfosalicylic acid for conversion of C₅/C₆ carbohydrates into ethyl levulinate. *React. Chem. Eng.* **2020**, *5*, 1759–1767. [CrossRef]
158. Zaccheria, F.; Scotti, N.; Ravasio, N. Solid Acids for the Reaction of Bioderived Alcohols into Ethers for Fuel Applications. *Catalysts* **2019**, *9*, 172. [CrossRef]
159. Zhao, D.; Prinsen, P.; Wang, Y.; Ouyang, W.; Delbecq, F.; Len, C.; Luque, R. Continuous Flow Alcoholysis of Furfuryl Alcohol to Alkyl Levulinates Using Zeolites. *ACS Sustain. Chem. Eng.* **2018**, *6*, 6901–6909. [CrossRef]
160. Islam, M.M.; Bhunia, S.; Molla, R.A.; Bhaumik, A.; Islam, S.M. Organic Solid Acid Catalyst for Efficient Conversion of Furfuryl Alcohol to Biofuels. *ChemistrySelect* **2016**, *1*, 6079–6085. [CrossRef]
161. Zhai, P.; Lv, G.; Cai, Z.; Zhu, Y.; Li, H.; Zhang, X.; Wang, F. Efficient Production of Ethyl Levulinate from Furfuryl Alcohol Catalyzed by Modified Zirconium Phosphate. *ChemistrySelect* **2019**, *4*, 3940–3947. [CrossRef]
162. Zhou, H.; Song, J.; Kang, X.; Hu, J.; Yang, Y.; Fan, H.; Meng, Q.; Han, B. One-pot conversion of carbohydrates into gamma-valerolactone catalyzed by highly cross-linked ionic liquid polymer and Co/TiO₂. *RSC Adv.* **2015**, *5*, 15267–15273. [CrossRef]
163. Zhao, G.; Liu, M.; Xia, X.; Li, L.; Xu, B. Conversion of Furfuryl Alcohol into Ethyl Levulinate over Glucose-Derived Carbon-Based Solid Acid in Ethanol. *Molecules* **2019**, *24*, 1881. [CrossRef] [PubMed]

164. Tian, H.; Shao, Y.; Liang, C.; Xu, Q.; Zhang, L.; Zhang, S.; Liu, S.; Hu, X. Sulfated attapulgite for catalyzing the conversion of furfuryl alcohol to ethyl levulinate: Impacts of sulfonation on structural transformation and evolution of acidic sites on the catalyst. *Renew. Energ.* **2020**, *162*, 1576–1586. [[CrossRef](#)]
165. Shao, Y.; Du, W.; Gao, Z.; Sun, K.; Zhang, Z.; Li, Q.; Zhang, L.; Zhang, S.; Liu, Q.; Hu, X.J. Sulfated TiO₂ nanosheets catalyzing conversion of biomass derivatives: Influences of the sulfation on distribution of Brønsted and Lewis acidic sites. *Chem. Technol. Biot.* **2020**, *95*, 1337–1347. [[CrossRef](#)]
166. Zhao, G.; Hu, L.; Sun, Y.; Zeng, X.; Lin, L. Conversion of Biomass-Derived Furfuryl Alcohol into Ethyl Levulinate Catalyzed by Solid Acid in Ethanol. *BioResources* **2014**, *9*, 2634–2644. [[CrossRef](#)]
167. Tiwari, M.S.; Gawade, A.B.; Yadav, G.D. Magnetically separable sulfated zirconia as highly active acidic catalysts for selective synthesis of ethyl levulinate from furfuryl alcohol. *Green Chem.* **2017**, *19*, 963–976.
168. Zhang, Z.; Yuan, H.; Wang, Y.; Ke, Y.J. Preparation and characterisation of ordered mesoporous SO₄²⁻/Al₂O₃ and its catalytic activity in the conversion of furfuryl alcohol to ethyl levulinate. *Solid State Chem.* **2019**, *280*, 120991. [[CrossRef](#)]
169. Shao, Y.; Li, Y.; Sun, K.; Zhang, Z.; Tian, H.; Gao, G.; Li, Q.; Liu, Q.; Hu, X. Sulfated Zirconia with Different Crystal Phases for the Production of Ethyl Levulinate and 5-Hydroxymethylfurfural. *Energy Technol. Ger.* **2020**, *8*, 1900951. [[CrossRef](#)]
170. Topolyuk, Y.A.; Nekhaev, A.I. Functionalized nanocarbon materials as catalysts for the ethanolysis of furfuryl alcohol. *Mendeleev Commun.* **2018**, *28*, 93–95. [[CrossRef](#)]
171. Guo, H.; Hirosaki, Y.; Qi, X.; Smith, R.L. Synthesis of ethyl levulinate over amino-sulfonated functional carbon materials. *Renew. Energ.* **2020**, *157*, 951–958. [[CrossRef](#)]
172. Wang, Y.; Zhao, D.; Triantafyllidis, K.S.; Ouyang, W.; Luque, R.; Len, C. Microwave-assisted catalytic upgrading of bio-based furfuryl alcohol to alkyl levulinate over commercial non-metal activated carbon. *Mol. Catal.* **2020**, *480*, 110630. [[CrossRef](#)]
173. Wu, J.; Shao, Y.; Jing, G.; Zhang, Z.; Ye, Z.; Hu, X.J. Design of graphene oxide by a one-pot synthetic route for catalytic conversion of furfural alcohol to ethyl levulinate. *Chem. Technol. Biotechnol.* **2019**, *94*, 3093–3101. [[CrossRef](#)]
174. Zhu, S.; Chen, C.; Xue, Y.; Wu, J.; Wang, J.; Fan, W. Graphene Oxide: An Efficient Acid Catalyst for Alcoholysis and Esterification Reactions. *ChemCatChem* **2014**, *6*, 3080–3083. [[CrossRef](#)]
175. Russo, P.A.; Antunes, M.M.; Neves, P.; Wiper, P.V.; Fazio, E.; Neri, F.; Barreca, F.; Mafra, L.; Pillinger, M.; Pinna, N.; et al. Mesoporous carbon–silica solid acid catalysts for producing useful bio-products within the sugar-platform of biorefineries. *Green Chem.* **2014**, *16*, 4292–4305.
176. Russo, P.A.; Antunes, M.M.; Neves, P.; Wiper, V.P.; Fazio, E.; Neri, F.; Barreca, F.; Mafra, L.; Pillinger, M.; Pinna, N.; et al. Solid acids with SO₃H groups and tunable surface properties: Versatile catalysts for biomass conversion. *J. Mater. Chem. A* **2014**, *2*, 11813–11824. [[CrossRef](#)]
177. Gao, X.; Peng, L.; Li, H.; Chen, K. Formation of Humin and Alkyl Levulinate in the Acid-catalyzed Conversion of Biomass-derived Furfuryl Alcohol. *BioResources* **2015**, *10*, 6548–6564.
178. Onkarappa, S.B.; Bhat, N.S.; Dutta, S. Preparation of alkyl levulinates from biomass-derived 5-(halomethyl)furfural (X = Cl, Br), furfuryl alcohol, and angelica lactone using silica-supported perchloric acid as a heterogeneous acid catalyst. *Biomass Convers. Biorefin.* **2020**, *10*, 849–856. [[CrossRef](#)]
179. Zhang, Z.; Wang, P.; Wu, Z.; Yue, C.; Wei, X.; Zheng, J.; Xiang, M.; Liu, B. Efficient synthesis of niobium pentoxide nanowires and application in ethanolysis of furfuryl alcohol. *RSC Adv.* **2020**, *10*, 5690–5696.
180. Skrodzky, K.; Antunes, M.M.; Han, X.; Santangelo, S.; Scholz, G.; Valente, A.A.; Pinna, N.; Russo, P.A. Niobium pentoxide nanomaterials with distorted structures as efficient acid catalysts. *Commun. Chem.* **2019**, *2*, 129. [[CrossRef](#)]
181. Ren, D.; Fu, J.; Li, L.; Liu, Y.; Jin, F.; Huo, Z.T. Efficient conversion of biomass-derived furfuryl alcohol to levulinate esters over commercial α -Fe₂O₃. *RSC Adv.* **2016**, *6*, 22174–22178. [[CrossRef](#)]
182. Chada, R.R.; Koppadi, K.S.; Enumula, S.S.; Kondeboina, M.; Kamaraju, S.R.R.; Burri, D.R. Effect of WO_x Doping into Pt/SiO₂ Catalysts for Glycerol Hydrogenolysis to 1,3-Propanediol in Liquid Phase. *Catal. Lett.* **2018**, *148*, 1731–1738. [[CrossRef](#)]
183. Lingaiah, N. One pot selective transformation of biomass derived chemicals towards alkyl levulinates over titanium exchanged heteropoly tungstate catalysts. *Catal. Today* **2018**, *309*, 269–275.
184. Neves, P.; Russo, P.A.; Fernandes, A.; Antunes, M.M.; Farinha, J.; Pillinger, M.; Ribeiro, M.F.; Castanheiro, J.E.; Valente, A.A. Mesoporous zirconia-based mixed oxides as versatile acid catalysts for producing bio-additives from furfuryl alcohol and glycerol. *Appl. Catal. A Gen.* **2014**, *487*, 148–157. [[CrossRef](#)]
185. Guo, Q.; Yang, F.; Liu, X.; Sun, M.; Guo, Y.; Wang, Y. Low-cost synthesis of nanoaggregate SAPO-34 and its application in the catalytic alcoholysis of furfuryl alcohol. *Chin. J. Catal.* **2020**, *41*, 1772–1781. [[CrossRef](#)]
186. Wang, M.-Y.; Su, H.; Zhai, G.-Y.; Yu, Q.-Y.; Wang, H.-H.; Jiang, Z.-D.; Li, X.-H.; Chen, J.-S. Synergy of B and Al Dopants in Mesoporous MFI Nanocrystals for Highly Selective Alcoholysis of Furfuryl Alcohol into Ethyl Levulinate. *Energy Technol. Ger.* **2019**, *7*, 1900271. [[CrossRef](#)]
187. Nandiwale, K.Y.; Pande, A.M.; Bokade, V.V. One step synthesis of ethyl levulinate biofuel by ethanolysis of renewable furfuryl alcohol over hierarchical zeolite catalyst. *RSC Adv.* **2015**, *5*, 79224–79231. [[CrossRef](#)]
188. Lange, J.-P.; van de Graaf, W.D.; Haan, R.J. Conversion of Furfuryl Alcohol into Ethyl Levulinate using Solid Acid Catalysts. *ChemSusChem* **2009**, *2*, 437–441. [[CrossRef](#)]
189. Cao, Q.; Guan, J.; Peng, G.; Hou, T.; Zhou, J.; Mu, X. Solid acid-catalyzed conversion of furfuryl alcohol to alkyl tetrahydrofurfuryl ether. *Catal. Commun.* **2015**, *58*, 76–79. [[CrossRef](#)]

190. Enumula, S.S.; Koppadi, K.S.; Gurrum, V.R.B.; Burri, D.R.; Kamaraju, S.R.R. Conversion of furfuryl alcohol to alkyl levulinate fuel additives over Al₂O₃/SBA-15 catalyst. *Sustain. Energy Fuels* **2017**, *1*, 644–651. [[CrossRef](#)]
191. Neves, P.; Lima, S.; Pillinger, M.; Rocha, S.M.; Rocha, J.; Valente, A.A. Conversion of furfuryl alcohol to ethyl levulinate using porous aluminosilicate acid catalysts. *Catal. Today* **2013**, *218*, 76–84. [[CrossRef](#)]
192. Neves, P.; Antunes, M.M.; Russo, P.A.; Abrantes, J.P.; Lima, S.; Fernandes, A.; Pillinger, M.; Rocha, S.M.; Ribeiro, M.F.; Valente, A.A. Production of biomass-derived furanic ethers and levulinate esters using heterogeneous acid catalysts. *Green Chem.* **2013**, *15*, 3367–3376. [[CrossRef](#)]
193. Nandiwale, K.Y.; Pande, A.M.; Bokade, V.V. HPW anchored Meso-HZ-5, a novel catalyst for selective synthesis of ethyl levulinate biofuel by alcoholysis of biomass-derived furfuryl alcohol. *Environ. Prog. Sustain.* **2018**, *37*, 1736–1742. [[CrossRef](#)]
194. Kong, X.; Zhang, X.; Han, C.; Li, C.; Yu, L.; Liu, J. Ethanolysis of biomass based furfuryl alcohol to ethyl levulinate over Fe modified USY catalyst. *Mol. Catal.* **2017**, *443*, 186–192. [[CrossRef](#)]
195. Song, D.; An, S.; Sun, Y.; Zhang, P.; Guo, Y.; Zhou, D. Ethane-Bridged Organosilica Nanotubes Functionalized with Arenesulfonic Acid and Phenyl Groups for the Efficient Conversion of Levulinic Acid or Furfuryl Alcohol to Ethyl Levulinate. *ChemCatChem* **2016**, *8*, 2037–2048. [[CrossRef](#)]
196. Song, D.; An, S.; Lu, B.; Guo, Y.; Leng, J. Arylsulfonic acid functionalized hollow mesoporous carbon spheres for efficient conversion of levulinic acid or furfuryl alcohol to ethyl levulinate. *Appl. Catal. B Environ.* **2015**, *179*, 445–457.
197. An, S.; Song, D.; Lu, B.; Yang, X.; Guo, Y.H. Morphology Tailoring of Sulfonic Acid Functionalized Organosilica Nanohybrids for the Synthesis of Biomass-Derived Alkyl Levulinates. *Chem. Eur. J.* **2015**, *21*, 10786–10798. [[CrossRef](#)]